End-of-degree project
Degree in Physics

Magneto-optics with Dark Plasmons in Hybrid Nanocavities
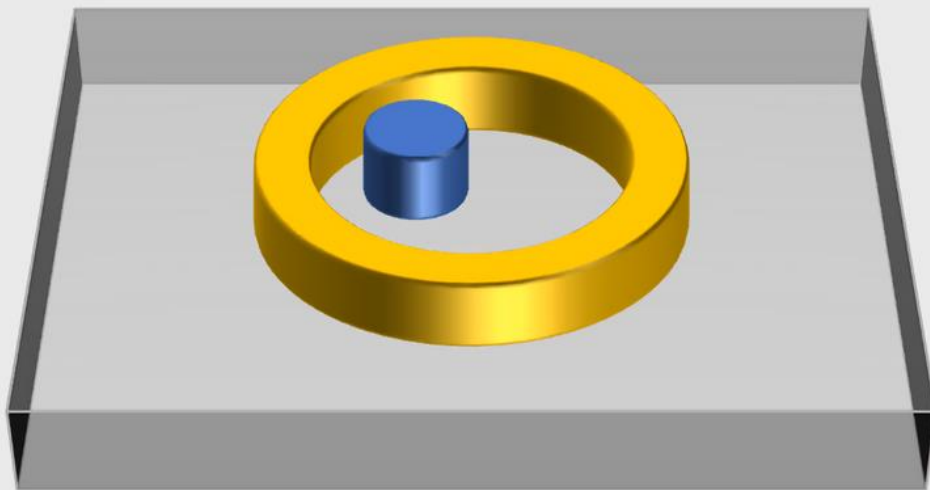
Author:
Mikel García Díez
Supervisor:
Prof. Paolo Vavassori

Faculty of Science and Technology. In association with the Nanomagnetism research group of CIC Nanogune (Spain)

Leioa, 19th June 2019

Abstract

Magneto-optics with Dark Plasmons in Hybrid Nanocavities

by Mikel García Díez

El Capítulo 1 es un resumen de los aspectos básicos de la magneto-plasmónica que introduce los conceptos más releventaes necesarios para entender el resto del texto.

En el Capítulo 2 mostramos que la actividad magneto-óptica de una nanoantenna en formato disco de permalloy es aumentada por encima del límite de una estructura simple mediante la excitación de un *modo oscuro* multipolar S_6 (debido a la simetría de la distribución de carga) de una nanocavidad en forma de anillo de oro cuando los dos componentes se colocan descentrados, formando un sistema híbrido. El modo dipolar brillante del componente ferromagnético se hibridiza con éste último para producir un modo dipolar *poco radiante* y otro dipolo *radiante* y amplificado gracias al acoplamiento espín-órbita en el permalloy en presencia de un campo magnético débil. Los resultados experimentales y las simulaciones por computador concuerdan en un aumento de un order de magnitud para el modo híbrido comparado a la resonancia dipolar pura del disco de permalloy por sí mismo.

A estos resultados los siguen en el Capítulo 3 cálculos por computador de discos con funciones dieléctricas modificadas para resonar a la misma longitud de onda que el modo S_6 que sugieren que un mayor aumento de la actividad magneto-óptica es posbible cuando las dos resonancias tienen lugar en el mismo punto espectral.

iv

Chapter 1 is summary of the basics of magneto-plasmonics that introduces the most relevant concepts necessary to understand the rest of the text.

In Chapter 2 we show that the magneto-optical activity of a permalloy disk nanoantenna is enhanced beyond the limits of a bare one by the excitation of a multipolar S_6 (due to the symmetry of charge distribution) *dark mode* of a gold ring nanocavitity when arranged in a non-concentric hybrid system. The dipolar bright mode of the ferromagnetic component hybridises with the latter to produce a *low-radiant* dipolar mode and a *radiant*, amplified dipole enabled by spin-orbit coupling in the permalloy in the presence of a weak magnetic field. Experimental results and computer simulations agree in an enhancement of one order of magnitude for the hybrid mode compared to the pure dipolar resonance of a standalone permalloy disk.

These results are followed in Chapter 3 by computer calculations of disks with modified dielectric functions that resonate in tune with the exact S_6 mode which suggest that a further augmentation of magneto-optical activity is possible when both resonances take place at the same spectral point.

Acknowledgements

Contents

List of Figures

List of Abbreviations

EBL	Electron Bbeam Lithography
HCL	Hole-mask Colloidal Lithography
MOA	Magneto Optical Activity
LSPR	Localised Surface Plasmon Resonance
RCP	Right Circularly Polarised (light)
LCP	Left Circularly Polarised (light)
SO	Spin Orbit
MOKE	Magneto Optical Kerr Effect
MOLPR	Magneto Optical Localised Surface Plasmon Resonance
QNM	Quasi Normal Mode
NCRD	Non-Concentric Ring and Disk
SEM	Scanning Electron MMicroscope
AFM	Atomic Force Microscope
EELS	Electron Energy Loss Spectroscopy
SFF	Scattered Field Formulation
FWHM	Full Width at Half Maximum

xii

0.1 Contexto y objetivos

0.1.1 Introducción

La nanotecnología es un área de investigación reciente debido a las complicaciones que impone en cuanto a fabricación y caracterización de estructuras en la nanoescala. Incluso hoy en día, con métodos sofisticados como la litografía por haz de electrones (EBL) y la litografía coloidal por huecos-máscaras (HCL), la precisión con la que pueden ser fabricados es limitada y requiere de cierta pericia.

Los sistemas en la nanoescala son la base perfecta para el desarrollo de nuevos materiales y tecnologías, pues muestran un comportamiento excepcional que dan lugar a fenómenos físicos que son inconcebibles en la macroescala. En este contexto, varias ramas del conocimiento confluyen.

La plasmónica está íntimamente relacionada a ella. Un campo electromagnético como la luz que incide sobre un sistema nanométrico puede excitar una *resonancia plasmónica*. Estas oscilaciones resonantes del gas de electrones de ciertos metales inducen un potente campo eléctrico en la vecindad de las nanoestructuras a través del apodado *confinamiento de la luz*. Con el objetivo de aprovechar características como la alta sensibilidad al medio en el que se encuentran, uno puede, por ejemplo, idear dispositivos que rastreen la presencia de ciertas moléculas en el entorno.

Una de estas posibles interacciones relaciona la plasmónica con la *magneto-óptica*. Algunos materiales, en concreto los metales ferromagnéticos, muestran la capacidad de cambiar la polarización de la luz que se transmite o refleja a través de ellos en los llamados efecto Faraday y Kerr, respectivamente, en presencia de un campo magnético. Es intuitivo pensar que un campo EM tan grande concentrado en un espacio tan pequeño por una resonancia plasmónica modificará y posiblemente aumentará estas propiedades, que pueden ser aplicadas en la creación de dispositivos ópticos como rotores en un factor de forma que era imposible hace unos años, dando lugar al área de investigación de la *óptica plana*, por ejemplo.

0.1.2 Objetivos

En el contexto de todas las mencionadas disciplinas, este trabajo de fin de grado tiene como meta profundizar en el estudio de estas interacciones analizando una estructura muy específica compuesta de un disco de permalloy (níquel y hierro) colocado dentro de un anillo de oro de 100 nanómetros. Tal sistema híbrido, con un metal ferromagnético y otro noble, aprovecha la interacción de los plasmones con los efectos magneto-ópticos y muestra una electrodinámica compleja que requiere un estudio riguroso. La novedad es que este aumento de la actividad magneto-óptica se consigue mediante la excitación de plasmones superficiales *localizados y poco radiantes*, rompiendo el límite preestablecido para esta amplificación. Esta tesis presentará resultados experimentales apoyados en simulaciones numéricas que aportan un entendimiento más profundo en la Física que tiene lugar entre los dos *nanómeros* y que resulta en un notorio aumento de la respuesta magneto-óptica en un sistema que no supera los pocos cientos de micrómetros de tamaño y tan solo unos nanómetros de espesor.

En la primera parte, el trabajo computacional sigue a los experimentos para intentar explicar lo que las nanoestructuras reales muestran y aportar datos que ayuden a entender los resultados mediante la resolución de las Ecuaciones de Maxwell. En la última parte de esta tesis, los métodos computacionales intercambian el lugar de guía con los experimentales para mostrar el camino determinando algunos

posibles materiales que podrían mostrar una respuesta mejor, evitando un gasto de tiempo y recursos en la realización de ideas que podrían no valerlos.

0.2   Context and aim

0.2.1   Introduction

Nanotechnology is a relatively new area of research due to the technical challenges it poses in terms of fabrication and characterization of such tiny structures. Even as of today, with sophisticated methods such as electron beam lithography (EBL) or hole mask colloidal lithography, the precision with which these are manufactured is limited and requires certain expertise. Nanoscaled systems are the perfect grounds for development of new materials and technologies, for they show exceptional behaviour that give way to physical phenomena that are not possible in the macroscale. In this context, several branches of knowledge come together.

Plasmonics is one of them. An electromagnetic field such as visible light impinging on a nanoscaled system can excite a *plasmon resonance*. These resonant oscillations of the electron gas in certain metals induce a very strong electric field in the vicinity of the nanostructures through the so-called *light confinement*. They store the electromagnetic energy of the incoming radiation in the near field, which gives raise to strong, interesting interactions that modify the optical properties of the material. Plasmonics aims to study the creation and control of these resonances and systems so small allow the excitation of plasmons in the visible spectrum of light. Exploiting features like the high sensitivity to surrounding media of the resonances, one can think of ultrasensitive devices that look for the presence of certain molecules, for example.

One of these possible interactions relates plasmonics to *magneto-optics*. Some materials, namely ferromagnetic metals, show the ability of changing the polarisation of the light that transmits through or reflects from them when a magnetic field polarises the samples. These are the magnetic Faraday and Kerr effect, respectively. It is intuitive to think that an enormous EM field concentrated in such a small space due to a plasmon resonance will modify, and hopefully enhance, these properties that can be applied to create optical devices such as rotators in a form factor that was not possible years ago, creating the research area of *flat optics* for example.

0.2.2   Objectives

In the context of all the former disciplines combined, this thesis aims to deepen the understanding of these interactions by studying a very specific nanostructure composed of a permalloy (nickel and iron) nanodisk placed inside a gold ring of few hundred nanometers. Such a hybrid system, with a ferromagnet and a noble metal, exploits the interplay of plasmons with magneto-optical effects and shows complex electrodynamics that require a rigorous study. The novelty in this work is that this augmentation of magneto-optical activity is achieved by the excitation of *localised and non-radiative* surface plasmons, breaking the pre-established limit for this amplification. This thesis will show experimental results supported by numerical simulations that provide deeper insight into the Physics that is happening between the two *nanomers* and result in a notorious enhancement of the magneto-optical response in a system that is no larger that few hundred micrometers and just a few nanometers thick.

In the first part, the computational work follows the experiments to try to explain what the real nanostructures show and provide useful data to understand these results through a numerical resolution of the Maxwell Equations. In the last part of this thesis, computational methods change roles with experimental procedures to lead the way in determining other possible materials that could yield a better result without the need of spending time and resources in realisation of ideas that are not worth them.

Chapter 1

Plasmonics and magneto-optics

In this chapter we provide an overview of the mechanism governing plasmon resonances, focusing on the type which is used in this very work, *localised surface* plasmon resonances (LSPRs). We will give a brief explanation of the Faraday and Kerr magneto-optic effects and, finally, we will tackle the interaction of these two phenomena.

1.1 Localised Surface Plasmon Resonances

1.1.1 The Drude and Drude-Lorentz models

The formalism which is commonly used to address the behaviour of the electrons in noble metals in the IR regime in plasmonics is the Drude model, developed circa 1900. The valence electrons of the atoms conforming the crystal are assumed to move freely with respect to the fixed ion cores, experimenting a collision approximately every time τ (typically 10^{-14} s at room temperature [1]). These events set the momentum of the electrons to a random direction and their kinetic energy according to the temperature of the area of the crystal it where it took place. The central equation for the mean linear momentum

$$\dot{\mathbf{p}} = -\frac{\mathbf{p}}{\tau} - e\mathbf{E}, \tag{1.1}$$

describes the motion between collision driven by an electric field $\mathbf{E}$. Unfortunately, the simplified model fails to account for features due to, for example, inter-band transitions. This is often mended by considering the response of bound electrons in lower-lying shells

$$m\ddot{\mathbf{x}} + m\gamma\dot{\mathbf{x}} + m\omega_0^2\mathbf{x} = -e\mathbf{E}, \tag{1.2}$$

for electrons of mass m, γ being the damping constant and ω_0 the natural frequency of oscillation. Assuming harmonic time-dependence for the electric field with frequency ω, one obtains the functional form of the dielectric permittivity

$$\varepsilon(\omega) = 1 - \frac{\omega_p^2}{\omega^2 + i\gamma\omega} + \sum_i \frac{A_i}{\omega_i^2 - \omega^2 - i\gamma_i\omega}, \tag{1.3}$$

where the summation has a term for every bound electron contribution with resonant frequency ω_i and damping γ_i we take into account and $\omega_p = \frac{ne^2}{\varepsilon_0 m}$ is the plasma frequency of the metal. For noble metals, $\omega_p \sim 2 \times 10^3$ THz and $\gamma \sim 10^{-2}$ eV [2]. This correction proposed in 1905 by Lorentz proves necessary when $\omega > \omega_p$, as the filled d band closed to the Fermi surface gives raise to a residual polarization due to

the ions cores $\mathbf{P}_\infty = \varepsilon_0(\varepsilon_\infty - 1)\mathbf{E}$ which must be added to the electronic contribution [3].

1.1.2 Localised plasmons

Quasi-static approximation

When discussing the excitation of localised surface plasmon resonances, one usually starts by considering a homogeneous sphere of diameter $2R << \lambda$. This approximation proves valid for describing the optical properties of nanoparticles not exceeding 100 nm. Since the impinging electric field does not vary spatially over the sphere, the problem is simplified. When placed in a non-absorbing medium (the electric permittivity ε_1 is real), homogeneous medium with an electric field $\mathbf{E_0} = E_0\hat{\mathbf{z}}$, the sphere polarises creating an internal field that decreases the field inside the particle, opposing to $\mathbf{E_0}$.

This standard electrostatics problem is tackled by solving the *Laplace equation* $\nabla^2\Phi = 0$ for the scalar potential which has the general solution in terms of the Legendre polynomials P_l for finite potentials at the origin [4]

$$\Phi_2(r,\theta) = \sum_{l=0}^{\infty} A_l r^l P_l(\cos\theta), \tag{1.4a}$$

$$\Phi_1(r,\theta) = \sum_{l=0}^{\infty} (B_l r^l + C_l r^{-l-1}) P_l(\cos\theta). \tag{1.4b}$$

We consider the following boundary conditions:

- at $r \longrightarrow \infty$, $\Phi_1 \longrightarrow -E_0 r \cos\theta$

- continuity of tangential components of $\mathbf{E}$ and normal of $\mathbf{D}$ at $r = R$

we arrive to the final result.

$$\Phi_2(r,\theta) = -\frac{3\varepsilon_1}{\varepsilon_2 + 2\varepsilon_1} E_0 r \cos\theta, \tag{1.5a}$$

$$\Phi_1(r,\theta) = \frac{\mathbf{p} \cdot \mathbf{r}}{4\pi\varepsilon_0\varepsilon_1 r^3} - E_0 r \cos\theta. \tag{1.5b}$$

Equation 1.5b shows that the field outside is the background plus one created by a (total) dipole induced in the sphere, defined as

$$\mathbf{P} = \varepsilon_0\varepsilon_1\alpha\mathbf{E_0} = 4\pi\varepsilon_0\varepsilon_1 R^3 \frac{\varepsilon_2 - \varepsilon_1}{\varepsilon_2 + 2\varepsilon_1} \mathbf{E_0} \tag{1.6}$$

where

$$\alpha = 4\pi R^3 \frac{\varepsilon_2 - \varepsilon_1}{\varepsilon_2 + 2\varepsilon_1}. \tag{1.7}$$

When light impinges on the small sphere, the oscillating electric field gives raise to a coherent oscillation of the conduction electrons. The motion is resonantly amplified when the *Frölich conidition* $\mathrm{Re}\,\varepsilon_2(\omega) = -2\varepsilon_1$ is satisfied, as the polarizability α increases enormously. Since this quantity is complex in general, the oscillation of electrons is not exactly in phase with the driving field. Below the frequency of resonance the dipole follows the field but beyond that point it is in anti-phase.

This resonance is characterised by the *absorption and scattering cross-sections*, which follow from the Optical Theorem [5].

$$\sigma_{sc}(\omega) = \frac{k^4}{6\pi}|\alpha(\omega)|^2 \tag{1.8a}$$

$$\sigma_{abs}(\omega) = k \operatorname{Im} \alpha(\omega) \tag{1.8b}$$

Mie Theory for bigger particles

The plasmonic response of the system under study in this thesis cannot be fully described by the quasi-static approximation, as the diameter of the rings surrounding the ferromagnetic disk is 450nm. The electric field inside the particle does vary spatially and as a consequence, retardation effects appear and so the polarization 1.7 must be corrected. The problem for larger particles is richer than the simplified one as higher order of plasmon resonances can take place: quadrupolar, hexapolar, octupolar, etc.

The formalism in the frame of Mie scattering theory here used was presented by Maier and Wokaun and assumes that the polarisation is still homogeneous inside the nanostructure [6]. Here, we present the result for the polarisability of a sphere.

$$\alpha_{MW} = \frac{3\varepsilon_1(\varepsilon_2 - \varepsilon_1)V}{3\varepsilon_1 + (1 - R^2k^2 - i\frac{2R^3k^3}{3})(\varepsilon_2 - \varepsilon_1)} \tag{1.9}$$

The term R^2k^2 yields the *dynamic depolarisation* which red-shifts the resonance at larger volumes, the term $\sim R^3k^3$ accounts for the radiation damping and the 1 in the denominator gives the static contribution as it dominates when $Rk \ll 1$.

Characterisation of the field

Under the assumption that we can treat the sphere as a dipole, the electric field has the following functional form [4]

$$\mathbf{E_{dipole}} = \frac{1}{4\pi\varepsilon_0}\left\{k^2(\mathbf{n}\times\mathbf{p})\times\mathbf{n}\frac{e^{ikr}}{r} + [3\mathbf{n}(\mathbf{n}\cdot\mathbf{p}) - \mathbf{p}]\left(\frac{1}{r^3} - \frac{ik}{r^2}\right)e^{ikr}\right\}. \tag{1.10}$$

In the far-field regime, $\mathbf{E}$ is a spherical wave given by

$$\mathbf{E_{FF}} = \frac{1}{4\pi\varepsilon_0}k^2(\mathbf{n}\times\mathbf{p})\times\mathbf{n}\frac{e^{ikr}}{r}, \tag{1.11}$$

whereas near the sphere the field is that of a static dipole, which does not radiate energy and decays as r^{-3}

$$\mathbf{E_{NF}} = \frac{1}{4\pi\varepsilon_0}[3\mathbf{n}(\mathbf{n}\cdot\mathbf{p}) - \mathbf{p}]\frac{1}{r^3}. \tag{1.12}$$

Contrary to the far-field, the near-field does not propagate. The region separating the two asymptotic cases is not as easily describable and is outside the purpose of this text.

1.2   Magneto-Optical effects: Kerr and Faraday

When a material is placed inside a magnetic field **H** it can be *optically active*, that is, it can change the polarisation of light passing through it. This can be understood in terms of the dichroism and birefringence caused by the Lorentz force that drives the oscillations of the bound electrons [7]. It can also be analysed in terms of the macroscopic susceptibility tensor, which acquires off-diagonal imaginary terms. Considering the bound electrons to be confined by a harmonic potential of elastic constant k, with a static magnetic field in the $\hat{\mathbf{z}}$ direction, the equation for the movement of such particles of mass m reads

$$m\ddot{\mathbf{r}} + b\dot{\mathbf{r}} + k\mathbf{r} = -e\mathbf{E_0}e^{i\omega t} - e\mu_0\dot{\mathbf{r}} \times \mathbf{H} \tag{1.13}$$

with $\omega_0 = \sqrt{k/m}$. Assuming time-harmonic dependence for $\mathbf{r}$ and using that $\mathbf{P} = -Ne\mathbf{r} = \varepsilon_0\chi\mathbf{E_0}$ for N bound electrons, one finds:

$$\chi_{11} = \chi_{22} = \frac{Ne^2}{\varepsilon_0 m} \frac{\omega_0^2 - \omega^2 + i\omega\gamma}{\left(\omega_0^2 - \omega^2 + \omega\gamma\right)^2 - 4\omega^2\omega_L^2} \tag{1.14a}$$

$$\chi_{12} = -\chi_{21} = \frac{Ne^2}{\varepsilon_0 m} \frac{-2j\omega\omega_L}{\left(\omega_0^2 - \omega^2 + \omega\gamma\right)^2 - 4\omega^2\omega_L^2} \tag{1.14b}$$

$$\chi_{33} = \frac{Ne^2}{\varepsilon_0 m} \frac{1}{\omega_o^2 - \omega^2 - i\gamma\omega} \tag{1.14c}$$

where ω_L is the Larmor frequency and $\gamma = \frac{b}{m}$. The wave equation for a dielectric medium can be then cast in the form [8]

$$\mathbf{\nabla} \times (\mathbf{\nabla} \times \mathbf{E}) + \frac{1}{c^2}\frac{\partial^2\mathbf{E}}{\partial t^2} = -\frac{1}{c^2}\chi\frac{\partial^2\mathbf{E}}{\partial t^2} \tag{1.15}$$

and for a plain wave given by $\mathbf{k}$, the following must be satisfied

$$\mathbf{k} \times (\mathbf{k} \times \mathbf{E}) + \frac{\omega^2}{c^2}\mathbf{E} = -\frac{\omega^2}{c^2}\chi\mathbf{E} \tag{1.16}$$

obtaining two independent solutions for the modulus k and the relation between the components E_x and E_y (E_z requiring to be zero)

$$k = \frac{\omega}{c}\sqrt{1 + \chi_{11} \pm \chi_{12}} \tag{1.17a}$$

$$E_x = \pm iE_y \tag{1.17b}$$

So it is clear that the $(+)$ sing must apply to *right-handed* circular light and the $(-)$ for *left-handed*. The expressions for the indices of refraction for said polarisations are

$$n_R = \sqrt{1 + \chi_{11} + \chi_{12}} \tag{1.18a}$$

$$n_L = \sqrt{1 + \chi_{11} - \chi_{12}} \tag{1.18b}$$

and make explicit the birefringence and dichroism that causes the change in polarisation. Note that the index is complex and it will then affect not only the plane of polarisation but the ellipticity, absorbing left and right-handed light in different amounts.

Faraday effect

To quantify the strength of the effect when the light goes through the sample, consider a linear light written in terms of the circular basis

$$E_0 \begin{bmatrix} 1 \\ 0 \end{bmatrix} e^{i(kz-\omega t)} = \frac{E_0}{2} \begin{bmatrix} 1 \\ -i \end{bmatrix} e^{i(k_R z - \omega t)} + \frac{E_0}{2} \begin{bmatrix} 1 \\ i \end{bmatrix} e^{i(k_L z - \omega t)} \qquad (1.19)$$

after traversing a distance *l*, both components will be out of phase

$$\frac{E_0}{2} \begin{bmatrix} 1 \\ -i \end{bmatrix} e^{ik_n l} + \frac{E_0}{2} \begin{bmatrix} 1 \\ i \end{bmatrix} e^{ik_L l} = E_0 e^{i\psi} \begin{bmatrix} \cos\theta \\ \sin\theta \end{bmatrix} \qquad (1.20)$$

defining

$$\psi = \frac{(k_R + k_L)l}{2} \qquad (1.21a)$$

$$\theta = \frac{(k_R - k_L)l}{2} \qquad (1.21b)$$

An important note is that the rotation of the direction of polarisation θ is *proportional* to the distance of propagation inside the active medium. This is one of the key aspects of magneto-plasmonics, as they yield a big effect in rotation in a sample that is very thin

Magneto-Optic Kerr effect (MOKE)
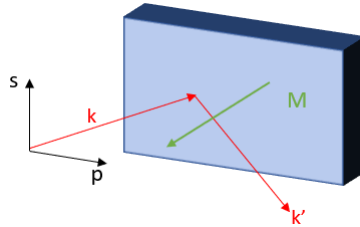
FIGURE 1.1: Polar MOKE geometry. Magnetization **M** is perpendicular to the surface. s and p designate the polarizations perpendicular and parallel to the plane of incidence, respectively, for a plane wave of propagation vector **k**.

The Kerr effect refers to the case where the light changes polarisation upon *reflecting* on the medium and it can be most conveniently described in terms of the Fresnel coefficient which is different for RCP and LCP light. Since wi well be dealing with (almost) normal incidence on the sample, it reads

$$r_{R,L} = -\frac{n_{R,L} - 1}{n_{R,L} + 1} = |r| e^{i\phi_{R,L}} \qquad (1.22)$$

this means that both polarisations acquire a different phase *and amplitude*, so linearly polarised X light like 1.19 will be modified

$$\frac{1}{2}E_0\left\{\begin{bmatrix}1\\i\end{bmatrix}\left(-\frac{n_L-1}{n_L+1}\right)+\begin{bmatrix}1\\-i\end{bmatrix}\left(-\frac{n_R-1}{n_R+1}\right)\right\}=\frac{E_0(1-n_Rn_L)}{(n_L+1)(n_R+1)}\begin{bmatrix}1\\i\left(\frac{n_R-n_L}{1-n_Rn_L}\right)\end{bmatrix}$$
$$=\frac{E_0(1-n_Rn_L)}{(n_L+1)(n_R+1)}\begin{bmatrix}1\\\theta_K+i\varepsilon_K\end{bmatrix}.$$
(1.23)

The total response, denominated *magneto-optical activity* (MOA) is the modulus of the complex Kerr angle

$$MOA=\sqrt{\theta_K^2+\varepsilon_K^2}$$
(1.24)

and accounts for both the rotation θ_K and change in ellipticity ε_K.

1.3   Magneto-plasmonics: interaction of LSPRs and MO effects

In the last decades, attention was turned towards the interplay of the plasmonic and magneto-optical effects, revitalised by the technological advance that enabled the fabrication of nanostructures supporting plasma resonances.

Normally, in order to exploit the best of both phenomena, one uses systems comprised of two types of material. On one hand, ferromagnets are best at showing strong MO effects due to the large magnetic susceptibility and the ability to attain magnetic saturation with a relatively small external field. Ferromagnetic materials happen to display stronger spin-orbit (SO) coupling and exchange interaction of electrons, as well as specific band features that improve the magneto-optical activity [9]. On the other hand, noble metals have rather lower optical losses and sustain LSPRs in the visible region of the EM spectrum. The sharp and strong plasmon resonances enhance the inherent MO activity, which is also modified by the plasmon supported by the ferromagnet itself, although weaker and broader.

Consider the matrix of Fresnell reflection coefficient

$$\begin{pmatrix}r_{pp}&r_{ps}\\r_{sp}&r_{ss}\end{pmatrix}.$$
(1.25)

The off-diagonal terms represent the conversion of p-polarised light into s-polarised. An external magnetic field produces extra-diagonal elements in the susceptibility 1.14, which in turn make r_{sp} and r_{ps} non-zero. The complex Kerr rotation (whose modulus is the MOA 1.24) measures the amount of impinging p-light that is being converted to s-polarised light

$$\phi_K=\theta_K+i\varepsilon_K=\frac{r_{sp}}{r_{pp}}$$
(1.26)

We will focus on the specific case of the ferromagnetic nanostructure being a nanodisk, which is the case of this very thesis. Not long ago, it was discovered that *two* LSPRs are excited when linear light shines upon the disk: one by direct interaction with the incoming field, and another one due to the SO coupling in the direction *orthogonal* to the former [10]. The proposed mechanism is two coupled harmonic damped oscillators, the magnetically activated one being the sole responsible for the

conversion of light polarisation in 1.26. Considering the dielectric tensor as a conse-
quence of the the external magnetic field to be, once the saturation of magnetisation
occurs

$$
\begin{pmatrix}
\varepsilon & -i\varepsilon Q & 0 \\
i\varepsilon Q & \varepsilon & 0 \\
0 & 0 & \varepsilon
\end{pmatrix}
\tag{1.27}
$$

where $Q = i(\varepsilon_{ij}/\varepsilon_{ii})$ is the *Voigt parameter*, ε_{xy} and ε_{yx} are linear in the magnetisation
m and account for the SO coupling. Linear light vibrating in the $\hat{x}$ direction induces
a dipole

$$
p_x = \chi_{xx} E_x^i = \varepsilon_0 (\varepsilon_r - \varepsilon_m) E_x^i
\tag{1.28}
$$

$E_x^i = E^0 - E_x^d$ being the difference of the incoming field and the depolarising one
inside the material. This can be put in terms of the original electric field

$$
p_x = \varepsilon_0 \alpha_{xx} E^0
\tag{1.29}
$$

The SO-coupling-activated dipole in the $\hat{y}$ direction will be

$$
p_y = \alpha_{yy} E_{SO} = \frac{\alpha_{yy} \varepsilon_{yx}}{\varepsilon - \varepsilon_m} E_x^i
\tag{1.30}
$$

and so the ratio between the two dipoles gives an expression for the Kerr angle, the
real part being θ_K and the imaginary ε_K

$$
\frac{p_y}{p_x} = \frac{\varepsilon_{yx} \alpha_{yy}}{(\varepsilon - \varepsilon_m)^2}
\tag{1.31}
$$

which is the polarization of the far field radiation in direction $\hat{z}$ by both oscillators
neglecting the feedback of p_y onto p_x.

One key aspect of the interaction of plasmonics with magneto-optics is that the
response can be tuned in different ways such as creating ordered lattices of the same
unit nanostructure or reshaping the systems to modify the spectral line of the MO
response by shifting the plasmon resonances [10][11].

Chapter 2

Overcoming the limits of MO activity enhancement

Equation 1.31 shows how one can augment the MOA in a nanoantenna, like the permalloy disks here mentioned, in a clear manner: enhancing the the dipole induced by the presence of the field (hereafter the Magneto-optical localised plasmon resonance, MOLPR) while keeping the optical one at bay, since it is the ratio of the two that gives the actual MO response of the system. Up until now, typical nanoantennas of Au or Ag have shown a *Q-factor* (which measures the sharpness of the resonance) of 10 approximately for the near-infrared (NIR) and visible range of electromagnetic radiation. The fact that both the optical and Magneto-optical dipoles are amplified poses an upper limit to the MOA one can achieve in a bare system. Indeed, the optical dipole-like LSPR of a nanodisk has an amplitude of $\sim Q$ times that of a continuous film whereas that of the MOLPR is augmented about Q^2 times. As a consequence, the MOA is amplified up to Q times or about one order of magnitude in the most favourable case.

The work here described aims to overcome this limitations by clever use of hybridisation of modes between a ring gold nanoresonator and a ferromagnetic disk nanoantenna that lies inside the first.

2.1 Cavity modes of a nanoring

We have already mentioned that ring-like nanostructures show a variety of cavity modes. A first distinction is made in terms of the way they can be excited. Most of these resonances are not excitable by linear light at normal incidence as their multipolar charge distribution forbids the coupling to a wave that vibrates in a plane only and retardation effects are ruled out by how the radiation approaches the ring [12]. Hence, in this conditions only two modes are visible: the dipolar *anti-bonding* and *bonding* [13] (Fig. 2.1), which are labelled as *bright modes*. There is however a plethora of remaining excitations, called *dark modes* in contrast to the former, that lie in the spectral range between the the strong dipolar ones and require other configurations to become activated. Moreover, as it is the case for the usual kind of nanostructures that have been studied, the spectral position at which these resonance occur can be modified, for a chosen material embedding medium, by varying the outer and inner radii or height, creating the possibility of tuning the optical response of the ring.

The contrast with the spectrum for a permalloy disk (or *dot*) array is clear. Ferromagnetic materials have a much weaker plasmonic response and the only dipolar resonance is very broad. Apart from this, the response of the ring lattice of pitch 800 nm is strong enough to produce diffractive coupling at two different wavelengths due to the presence of a substrate ($n = 1.5$) and air ($n = 1$). This effect is not seen
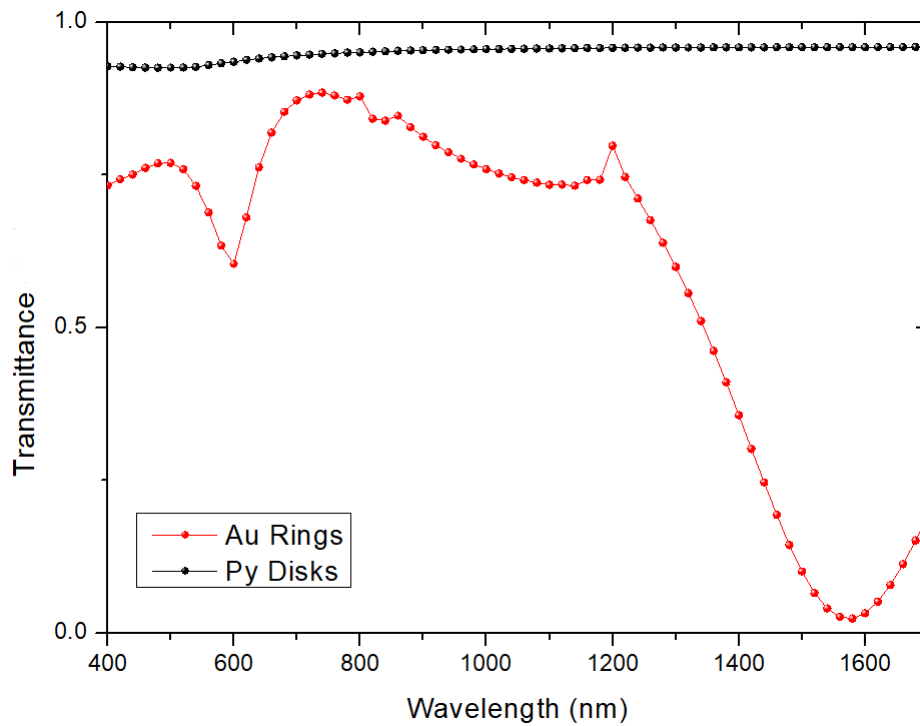
FIGURE 2.1: Transmittance spectra calculated separately for a gold ring lattice (red) and permalloy disk array (blue). 2 dips appear accounting for the absorption of energy for driving dipolar resonances. The plasmonic response of the ferromagnetic disks is substantially weaker and shows a very broad resonance. Features at 800 nm and 1200 nm correspond to diffractive couplings of the lattice through the air ($n = 1$) and the substrate ($n = 1.5$).
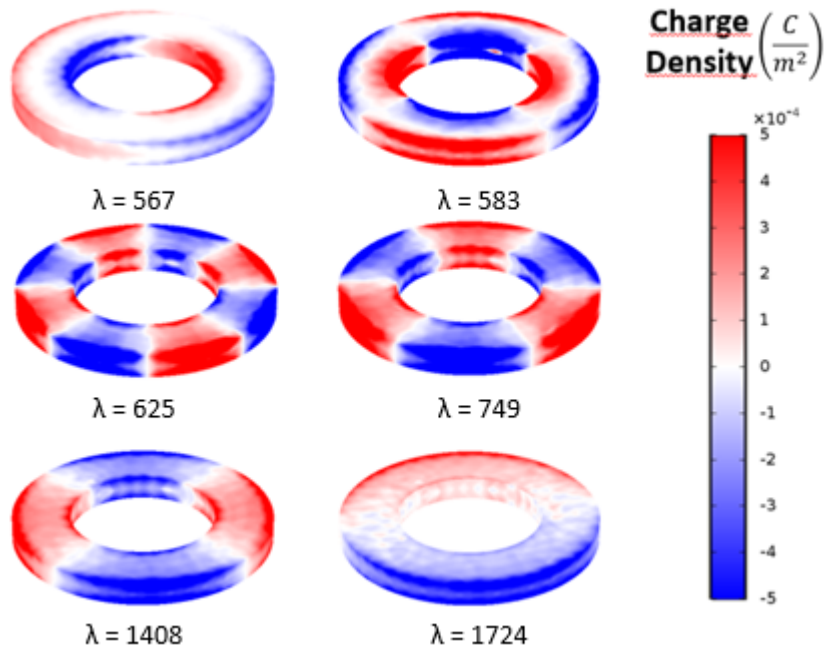
FIGURE 2.2: Computed charge distribution of eigenmodes for a ring of radii $R_i = 125$ nm and $R_o = 225$ nm in a uniform embedding medium of refractive index $n = 1.3$.

in experimental measurements, probably due to the imperfections of the real structures, and it is neglected.

As a first task, one has to study the nature of these multipolar modes in order to understand the dynamics involved. To do this, supported by the literature already present, we have conducted both computational simulations and experiments to contrast the results obtained by numerical procedures. An analysis of the eigenmodes can be performed in COMSOL Multiphysics using the tools that Yan et al. kindly provide (refer to text [14] for a detailed explanation). The application allows us to define the geometry of a ring of inner and outer radii $R_i = 125$ nm and $R_o = 225$ nm and use the parameters found in the literature [15] to define the optical properties based on a Lorentz-Drude model and compute the frequencies at which a resonances are found.

Figure 2.2 shows the the charge distribution for the normal modes in our range of interest which is calculated by plotting the normal component of the polarisation vector to the surface of the ring. Dipolar modes appear at 567 nm (anti-bonding) and 1724 nm (bonding) the rest being the aforementioned dark modes. A key difference is that the latter are *low-radiant*, meaning that less light is emitted back which causes lower radiative losses and a narrower resonant peak [16]. The existence of these cavity modes is vastly proved and here we include an experiment of electron energy loss microscopy that shows peaks in the expected positions accounting for the presence of strong fields near the resonator in a resonance regime (please note that these is an array of rings of different dimensions than those in Fig. 2.2 grown onto a SiN_2 membrane). The equipment used for this purpose was a TitanG2 60-300 (FEI, Netherlands) in monochromatic mode at 80 kV (energy resolution 80 meV as FWHM of ZLP).

It is worth noting that, although the procedure used to obtain images like Fig
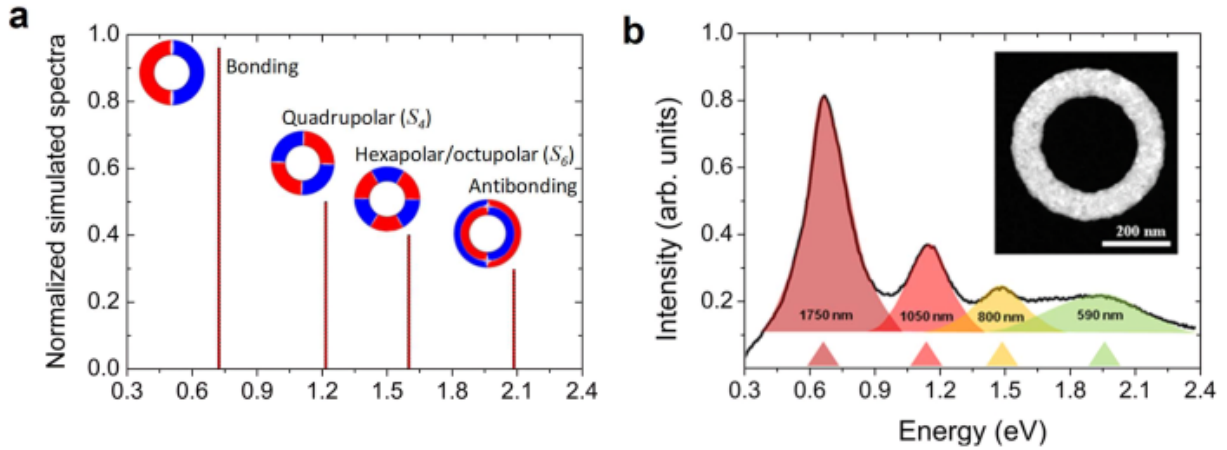
FIGURE 2.3: a) Computed spectral positions of 4 modes of a gold nanoring b)EELS spectrum for an order square array of gold rings with an estimation of the widths of the resonances. The inset is an scanning electron microscope (SEM) image of one ring in the lattice.
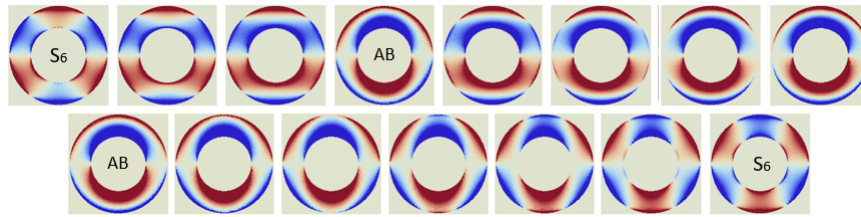
FIGURE 2.4: Charge distribution at $\lambda = 750$ nm computed through normal component of polarisation vector for gold rings in a square lattice of periodicity 1000 nm. Ring dimensions are: $r_{in} = 125$ nm and $r_{out} = 225$ nm and thickness of 40 nm. Starting from an arbitrary phase, each image represents a step of $\pi/15$ radians, completing half a period. Predominant contributions of the octupolar (S_6) and anti-bonding (AB) modes are visible.

2.2 conveniently isolates every normal mode from the other, this is not the real picture when a plane wave excites the resonances. Rather, at a specific wavelength, a convolution of modes will be seen and the contribution from each mode will be determined by the amplitude of resonance in that exact position in the spectrum (Fig. 2.4). For this physical situation we use standard *ports formulation* in frequency domain of the COMSOL software, which allows us to define periodic conditions to model a square array of unit cells which contain a centred gold ring of the same dimensions as those in Fig. 2.2 with periodicity of 1000 nm (this moves the diffractive coupling features in transmission and reflections to 1000 nm and 1500 nm so they do not interfere with the modes present in the range). We define the optical behaviour by implementing the data provided by Johnson and Christy [17], keeping in mind that these correspond to bulk properties and may cause a slight disagreement with experiments. The medium recreates that of the real samples, i.e., a SiN_x substrate of refractive index ≈ 1.5 with the structures exposed to open air (index 1). Data manipulation for figure 2.4 is done in a *Mathematica* notebook by taking the data for the normal polarisation vector (a complex number) and advancing the phase to reflect how the charge distribution evolves in time, eventually plotting only the real part. At $\lambda = 750$ nm, The most prominent contributions are from the octupolar (S_6, due to the improper rotation symmetry of the charge distribution) and the anti-bonding
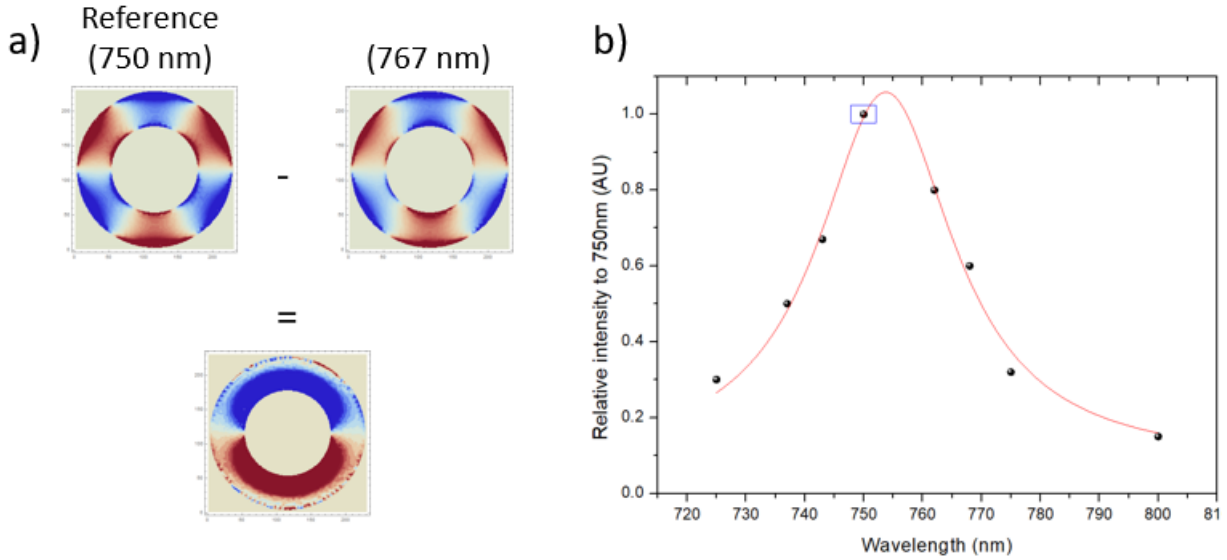
FIGURE 2.5: Study of width of octupolar resonance in a gold nanor-ing array (pitch 1000 nm, $R_i = 125$ nm and $R_o = 225$ nm) a) Example of procedure for obtaining the data in b), the relative amplitude compared to the reference at 750 nm (blue rectangle) fitted to a Gaussian function.

hinting at the existence of a non vanishing amplitude of this last normal mode even outside the resonant peak.

2.1.1   Octupolar (S_6) mode

With the idea of increasing the ratio of the magneto-optical and optical dipoles of the disk which will be placed inside the ring, dark modes constitute a good starting point due to their low-radiant nature. We turn our attention to the oc-tupolar/hexapolar (according to previous publications). This mode, as we will see, strongly couples to the dipole of the disk and hence is of utmost interest for the aim of this research.

One can estimate the width of this resonance by manipulating the data for the normal polarisation using the method of Fig. 2.4. With a wavelength fixed as a reference where the S_6 mode appears the strongest, we go through all the surrounding points shifting the phase until the S_6 symmetry clearly appears and subtract to that dataset the reference multiplied by a factor less than 1 (corresponding to the relative intensity at that point) until the contribution from the octupolar resonance vanishes (Fig 2.5a). A sensible curve for the resonance is obtained by performing a Gaussian fit to the data showing that this particular mode extends to at least 50 nm away from the peak amplitude (Fig. 2.5b) hence further reinforcing the idea that at a certain wavelength, various modes contribute with different amplitudes which result in the way the final charge distribution behaves.

2.2   Non-concentric ring-disk (NCRD) magnetoplasmonic system

The core of this work is the combination of magneto plasmonic nanoantennas and nanocavities. Usually, plasmonic nanocavities are synthesised with non-magnetic
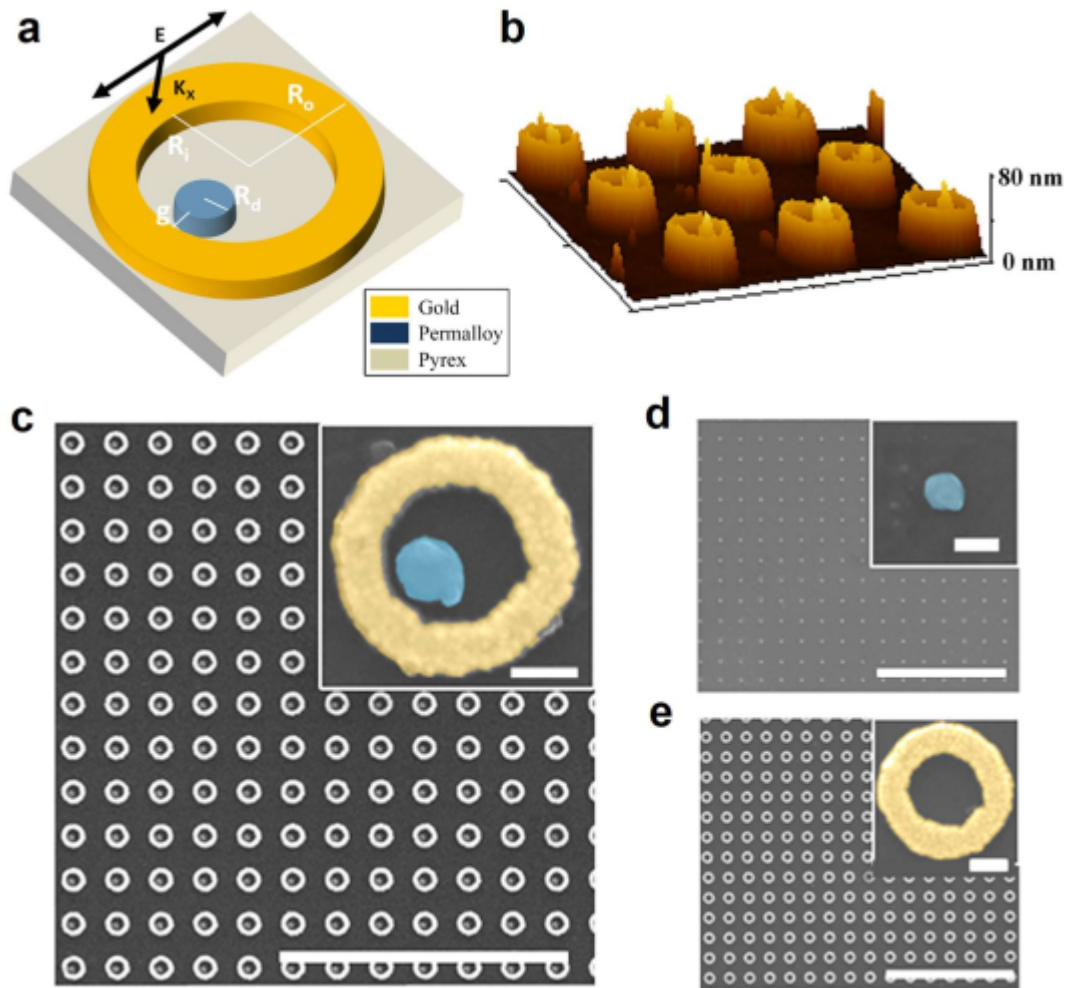
FIGURE 2.6: Characterisation of Py disks and Au rings and their arrangement in a NCRD structure. a) Schematic of NCRD with geometrical parameters and plane wave excitation characteristics. b) Atomic force microscope (AFM) image of NCRD array. c) Scanning electron microscope (SEM) image of the NCRD array and d) disk and e) gold by themselves.

materials such as gold or silver. Here, the use of a ferromagnetic permalloy disk-like nanoantenna inside a gold ring is proposed to exploit the interaction of the cavity modes sustained by the latter that will interact with the dipolar resonances in the permalloy disk. The excitation of the dark modes is allowed in this case by breaking the circular symmetry that both components (or even their concentric arrangement) have, as previous research proves possible [18]. The sample that was used to make the following experiments was a square array of non-concentric ring-disk (NCRD) system of periodicity 780 nm. The gold ring has radii $r_{in} = 130$ nm and $r_{out} = 215$ nm and the disk inside is placed off-centre leaving a gap of $g \approx 10$ nm, its radius being 50 nm. Both components are 40 nm thick. They were fabricated by electron-beam (e-beam) lithography and lift-off procedure. First, a 5 nm thick Ti layer was e-beam evaporated (evaporation rate: 0.4 Å/s) onto a cleaned 10 mm x 10 mm Pyrex substrate, as an adhesion layer and as a metallic coating for avoiding charging effects during e-beam lithography. The NCRD structures have been grown by a sequential two-step procedure. First, the Py disk was prepared by spin-coating a positive resist (ZEP520A-7) onto the substrate at 4000 rpm for 60 s. The resist was exposed by a 20 KV electron beam inside a RAITH eLine system. Exposition time was adjusted according to the disk size. After developing the exposed resist (with ZED-N50 developer), a 40 nm thick Py layer was thermally evaporated (evaporation rate: 0.8 Å/s). Finally, the lift-off was carried out by dipping the samples in the proper solvent (ZDMAC). The process was repeated in order to grow the gold rings around the dots.

Sample characteristics are presented in figure 2.6. SEM images where obtained through a eSEMFEI QuantaTM 250 microscope at an accelerating voltage of 10 kV and for AFM images a Nano Observer system (CSI Company, France) was used in air under ambient conditions. The slightly irregular form of the structures, given the challenging fabrication process, may justify the loss of fine details compared to simulations such as lattice diffractive coupling.

Although essential information is given on the numerical simulations, we refer the reader to Appendix A for more technical details.

2.2.1 Optical properties

We look at the transmittance spectra in order to analyse the plasmonic resonances in the parent structures and the NCRD system and study their optical properties. Figure 2.7b shows the experimental data recorded with an optical microscope for the samples described above and the computed counterpart obtained in COMSOL's *port formulation* (Fig. 2.7a) in excellent agreement. The disk spectrum shows a very broad plasmon (FWHM≈ 300 nm) centred at about 550 nm, which restricts the interaction with the ring to the anti-bonding and the near cavity modes. The resulting spectrum for the NCRD (in blue) is that of the stand-alone ring but with a very striking difference: a new peak appears at ∼ 820 nm owing to the only observable interaction among the various dark modes in the ring. Inspection of the surface charge distribution shows that this new resonance corresponds to the excitation of the S6 cavity mode, which is activated by the rupture of symmetry that placing the disk off-centred creates. The charge distribution has no longer the sixfold rotation symmetry but it is slightly distorted by the interaction with the dipole created in the dot. The latter is in turn modified by creating an uneven distribution of charge but conserving the dipolar character. It is remarkable that a appreciable signal is recorded even with a surface *filling factor* of about 1.2%.

FIGURE 2.7: Transmittance spectra of gold rings, Py disks and NCRD arrangement in the visible range. a) Computed. Inset shows full calculated range. b) Experimental. The dashed lines mark anti-bonding and S_6 resonances. The black arrow points at a feature product of the diffractive lattice coupling (only in simulations). c) Normalised charge distributions for marked resonances and plane of oscillation of incoming wave.

2.2.2 Magneto-optical enhancement

We further investigate this new interaction between the dot and the ring. Experiments are conducted using a Kerr spectrometer (Fig. 2.8a). An electromagnet creates a magnetic field **H** perpendicular to the sample that achieves the saturation magnetisation (350 mT) by switching between ±700 mT. Almost monochromatic light from a supercontinuum laser (SuperK Extreme EXR-15 from NKT Photonics) is linearly polarised and focused through a photoelastic modulator (Hinds Instruments II/FS42A) and impacts on a Si-photodetector (Thorlabs PDA 36A-EC) upon reflecting on the sample. By providing a reference signal at 42 kHz, the modulator allows the recording of both rotation (θ_K) and ellipticity (ε_K) at the reference frequency and twice that value respectively, achieving a standard deviation of 2 µrad. Finally, the data from orientation $-$**H** is subtracted to that of $+$**H** (keeping in mind that values should be equal in magnitude but opposite in sign) automatically by the experimental setup's software. Consequently, absolute values correspond to double the real quantities, which does not hinder the ability to compare them and measure the relative amplification. Numerical computations are adjusted to adapt to this fact.

Simulations are made this time, in standard COMSOL *scattered field formulation* (SFF). This method of modelling *single nanostructures* is used based on the agreement with experimental results and justified by assuming that diffractive coupling is negligible in our case. To implement the effect of the external magnetic field, the software allows the definition of the dielectric tensor in eq. 1.27 as

$$
\begin{pmatrix}
\varepsilon_d(\omega) & \mp\varepsilon_{od}(\omega) & 0 \\
\pm\varepsilon_{od}(\omega) & \varepsilon_d(\omega) & 0 \\
0 & 0 & \varepsilon_d(\omega)
\end{pmatrix}
$$

by manually inserting the tabulated values of the diagonal and off-diagonal terms for Ni from the reference [19]. The use of nickel is justified as it shares almost the same optical and MO properties as permalloy. The change of sign of the off-diagonal terms accounts for the inversion of orientation of **H**. To compute θ_K and ε_K, the integrated values of the incoming E_y and rotated E_x fields over a finely meshed area surrounding the structure are used in the expressions [20]

$$
\theta_K = \frac{\mathrm{Re}(E_y)\,\mathrm{Re}(E_x) + \mathrm{Im}(E_y)\,\mathrm{Im}(E_x)}{\mathrm{Re}(E_y)^2 + \mathrm{Re}(Ex)^2} \tag{2.1a}
$$

$$
\varepsilon_K = \frac{\mathrm{Re}(E_y)\,\mathrm{Im}(E_x) - \mathrm{Im}(E_y)\,\mathrm{Re}(E_x)}{\mathrm{Re}(E_y)^2 + \mathrm{Re}(Ex)^2} \tag{2.1b}
$$

$$
MOA = \frac{|E_x|}{|E_y| + R_{subs}} \tag{2.1c}
$$

where R_{subs} is the Fresnel coefficient at normal incidence of the substrate, whose contribution to the reflected field in original polarisation must be taken into account (typically it is calculated to be 0.2 approximately to fit the data). Figure 2.8c shows a striking enhancement over the MOA of the stand-alone disk of 6x where the interaction with the S$_6$ mode occurs even well beyond the maximum of plasmonic resonance of the dot. Both ellipticity and rotation curves are completely reshaped and amplified. The rotation increases as we approach the resonant wavelength, leading to a vanishing at that exact point where ellipticity, in turn, is maximised. These features are attributed to the hybridisation of the octupole in the ring with the dipole induced in the dot. The process is described as a *Fano interference* [21], in which
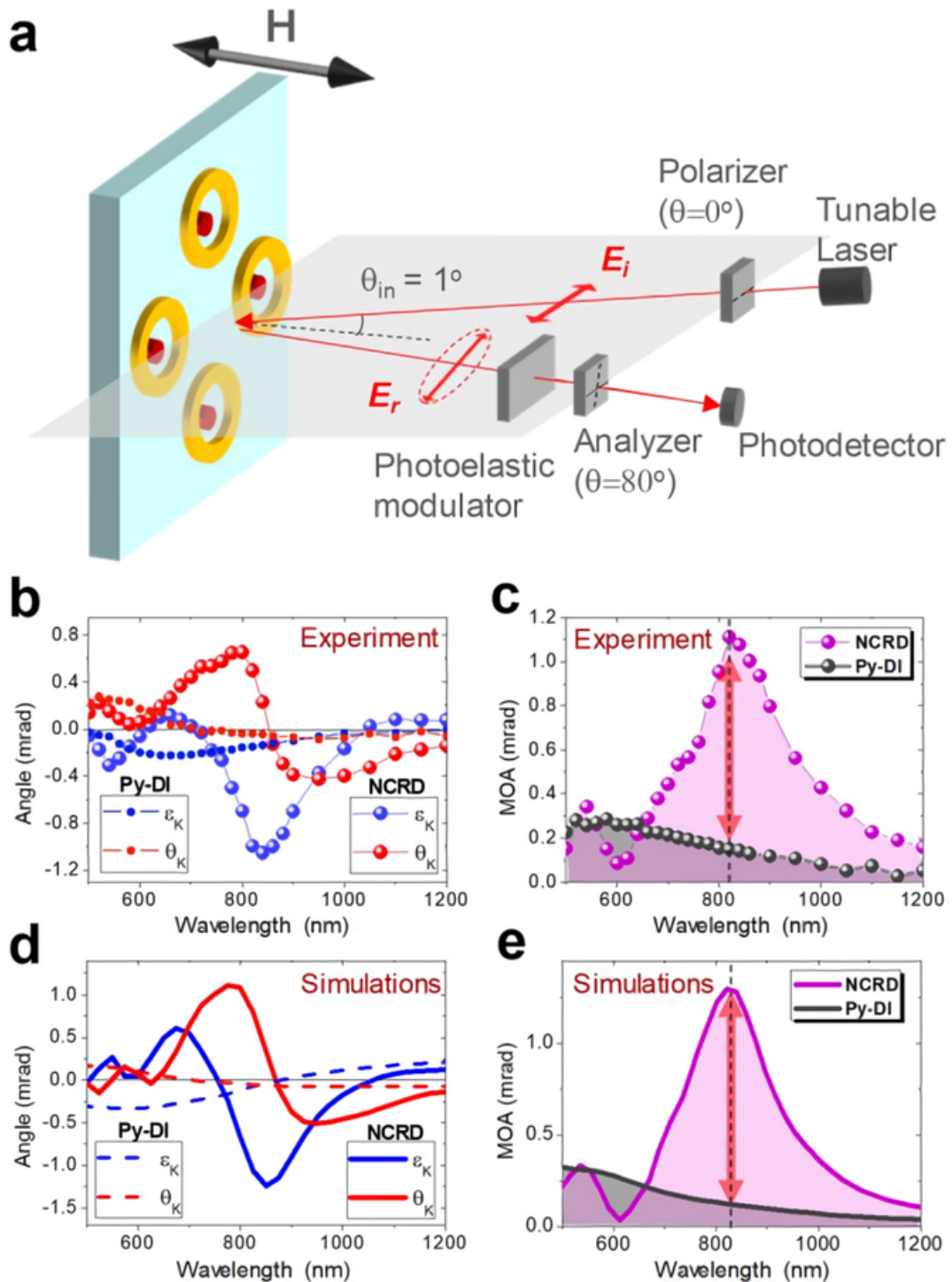
FIGURE 2.8: Measurement of magneto-optical response of NCRD system. a) Schematic of experimental setup. Rotation and ellipticity change for b) experiments d) simulations. Measurement of MOA for NCRD (pink) and disk alone (grey) in c) experiments and e) simulations.

a sharp and rapidly varying resonance (from the ring) interacts with another one which is broader (disk). We make clear that gold does not contribute to the MO signal appreciably given that the magnetic field used to magnetise the sample is not very strong so the amount of sheer magneto-optical material is exactly the same as it would be for an array of only disks with the same dimensions

Continuing with the model of two orthogonal harmonic oscillators, we investigate the magnitude of both associated dipoles ($\mathbf{p_O}$ and $\mathbf{p_{MO}}$) in the disk through the surface charge, to which they are proportional. Subtracting the the contribution of the optical part computed as the normal component of the polarisation $\sigma = \mathbf{p} \cdot \hat{\mathbf{n}}$ reveals the charge distribution for the SO-activated MOLPR. The data shows an amplification of the maximum of the surface charge $|\sigma|$ of approx. 1 order of magnitude at the $\lambda = 820$ nm resonance even compared to that of the stand-alone dot at its peak ($\lambda = 550$ nm) (Fig. 2.9). The enhancement is even stronger compared to the bare nanoantenna at $\lambda = 820$ nm, as the strength at that point is $\approx 20\%$ lower than at full resonance.

Further analysis of the charge distribution in both the disk and the near part of the ring reveals the true mechanism underlying the strong enhancement of MOA. By taking the surface charge density charts of the NCRD and subtracting that of the ring with the clear S_6 symmetry, we are left with the isolated contribution of a *coupled dipolar mode* whose associated dipole $\mathbf{p_C}$ can be decomposed into dipoles $\mathbf{p_h}$ and $\mathbf{p_O}$ taking place at the ring and disk respectively (Fig. 2.10a). This mode induced by the proximity of the two structures couples with the octupolar and creates the final effect. We can track the time evolution of the averaged surface charge in a tiny area of the ring and the disk (marked with star symbols in Fig. 2.10a). The analysis reveals that both $\mathbf{p_O}$ and $\mathbf{p_h}$ oscillate in phase which means that its interference must be constructive. The subsequent amplification of the optical dipole is transferred to the orthogonal magneto-optical one in the ferromagnetic disk, which simulations show that is not at all disturbed by the presence of the cavity modes.

Referring again to eq. 1.31, the mechanism that is responsible for the strong enhancement of MOA seems to be now clear. Not only is $\mathbf{p_{MO}}$ largely amplified due to the constructive interference that enhances the optical one but, we can think that, given the uneven charge distribution that $\mathbf{p_C}$ shows, the optical coupled mode hybridised with the S_6 resonance is *low-radiant*. This means that the denominator in eq. 1.31 is not as amplified as the numerator, which corresponds to the $\mathbf{p_{MO}}$ dipole and remains *radiant* in character since it does not hybridise. It is the combined effect of amplification of the MOLPR and the low-radiance of the optical one that increases that ratio enormously and yields the observed results.

This hypothesis is backed by three results. First, reflectivity measurements and calculations show that this quantity is marginally enhanced in the NCRD system with respect to the bare rings, pointing at the low radiant character of the hybrid mode (Fig. 2.10b). By using COMSOL's *scattered field formulation* one can compute the absorption cross-section of both systems. The comparison shows that the little enhancement of reflectivity is due to the energy being absorbed into the NCRD structure instead of reflected (Fig. 2.11b). In second place, coupling with the anti-bonding mode at $\approx$600 nm should yield a similar result which is not the case (Fig. 2.8c and e). This can be attributed to the superradiant character of the AB resonance, which fails to increase the ratio of light radiated in rotated and original polarisation as the S_6 does. Lastly, comparison to the concentric ring-disk (CRD) system shows that when symmetry is not broken, the octupolar mode may not be excited and the response is that of the bare ferromagnetic nanoantenna, neglecting minute discrepancies caused by the imperfections in the array fabrication (Fig. 2.12).
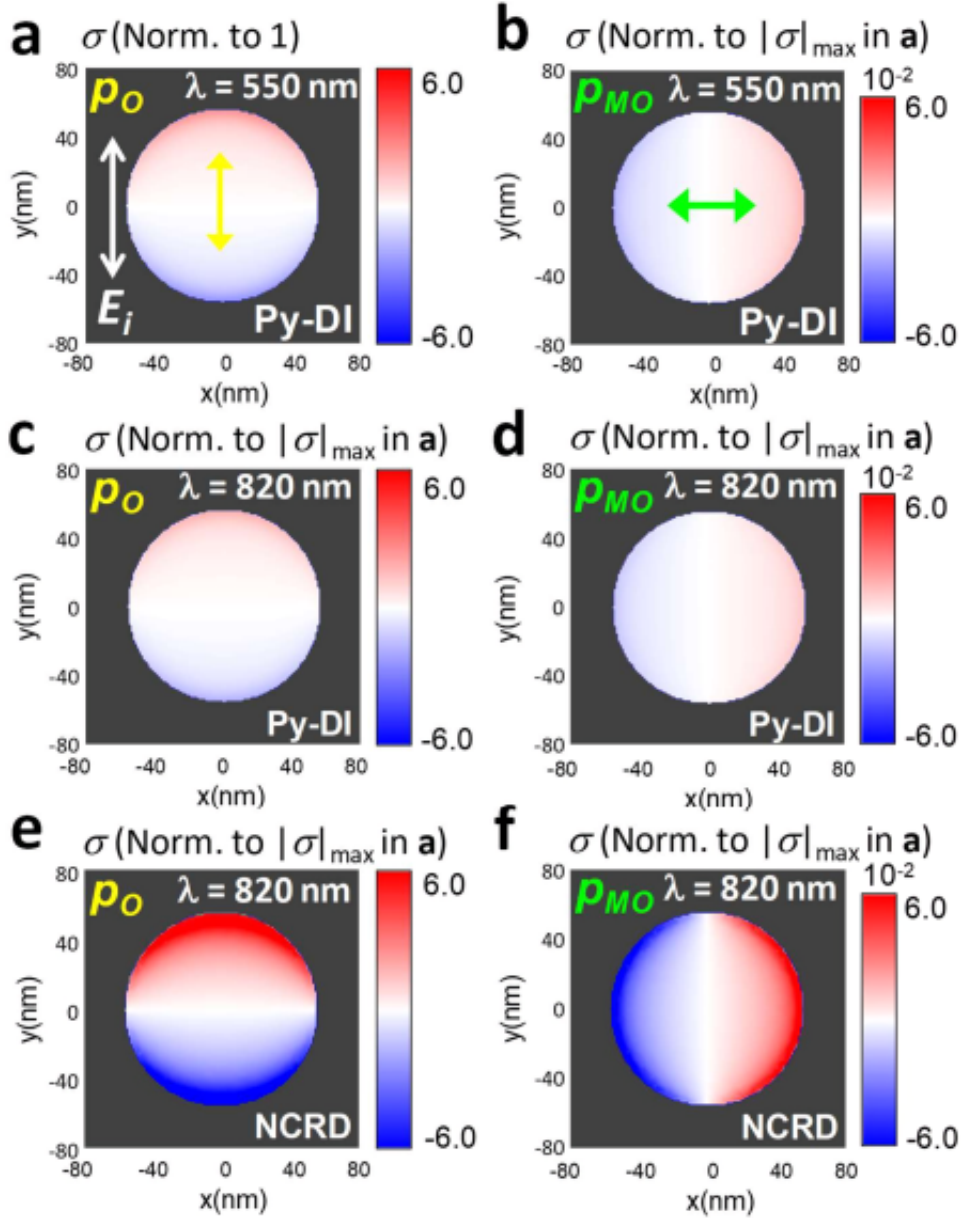
FIGURE 2.9: Surface charge for optical LPR ($\mathbf{p_O}$) and MOLPR ($\mathbf{p_{MO}}$) for disk at a) and b)$\lambda = 550$ nm; c) and d) $\lambda = 820$ nm; e) and f) NCRD at $\lambda = 820$ nm. White arrows shows the direction of oscillation of the incoming field E_i of $1\,\mathrm{V\,m^{-1}}$. Yellow and green arrows mark the direction of oscillation of $\mathbf{p_O}$ and $\mathbf{p_{MO}}$ respectively. Colour scaling is kept constant throughout the figure to show how sub figures compare.
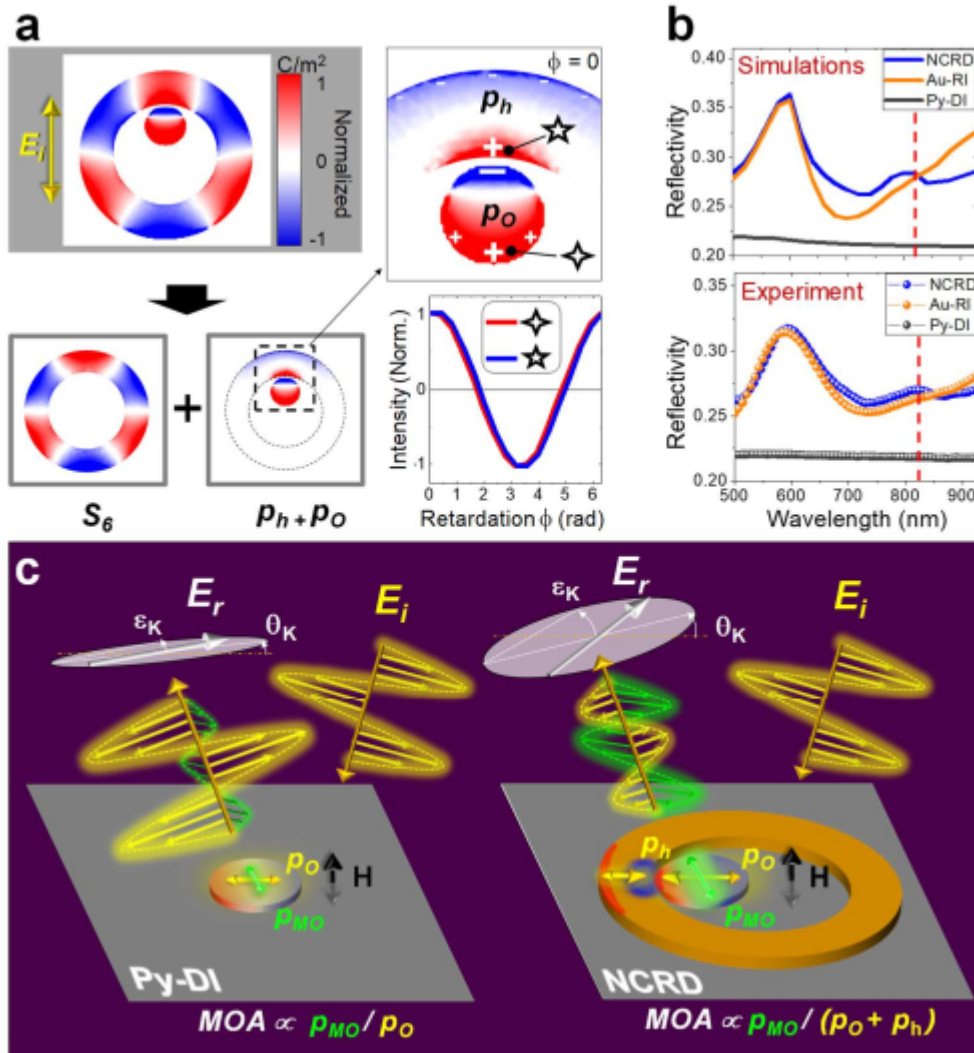
FIGURE 2.10: a) Decomposition of NCRD mode at $\lambda = 820$ nm into S_6 and coupled dipoles $\mathbf{p_h}$ and $\mathbf{p_O}$. Plot shows the time evolution of the charge in points marked with stars, which result to be in phase. b) Reflectivity simulations and measurements for stand-alone Py disks, Au rings and NCRD hybrid system. c) Pictorial representation of the mechanism governing the enhancement of MOA signal. E_i and E_r are the incoming and reflected fields. Yellow and green represents original and rotated polarisation. ε_K and θ_K are the ellipticity and rotation angles. The magnetic field $\mathbf{H}$, in black, is perpendicular to the sample. Red and blue represent accumulation of net positive and negative charge.
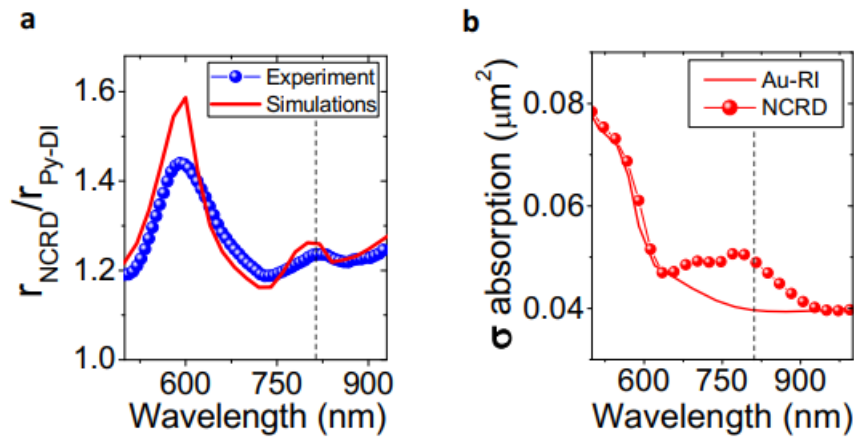
FIGURE 2.11: a) Ratio of reflectivity in NCRD and Py disks structures near AB and S_6 cavity modes. b) Absorption cross-section of NCRD and Au ring systems.
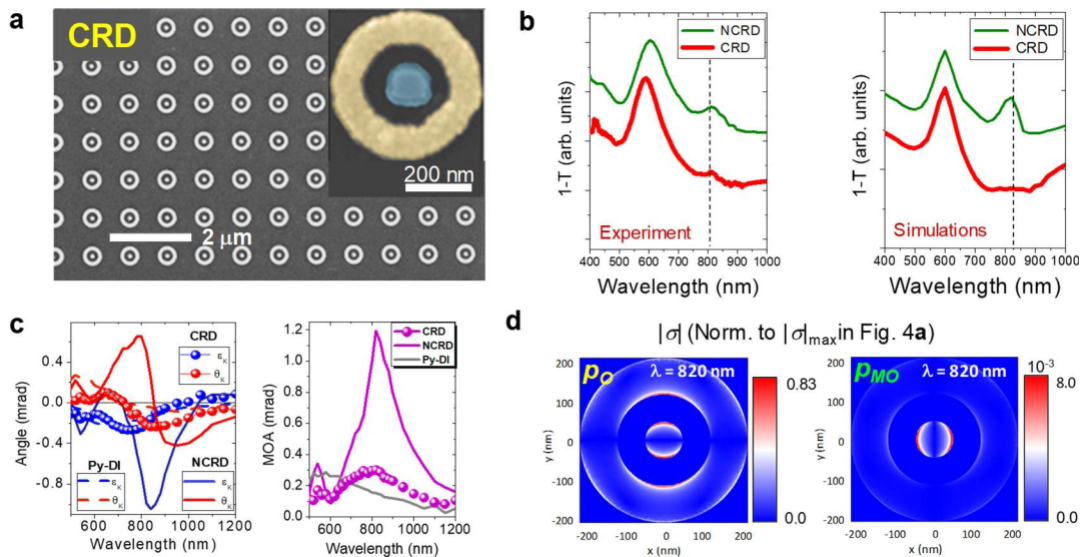
FIGURE 2.12: a) SEM images of CRD systems of the same nominal characteristics of NCRD counterpart. b) 1-T (transmittance) comparison between CRD and NCRD, both experimental and computed. c) Ellipticity and rotation angles and MOA of CRD, NCRD and Py disk. d) Optical ($\mathbf{p_O}$) and magneto-optical ($\mathbf{p_{MO}}$) dipole representation through $\sigma = \mathbf{p} \cdot \hat{\mathbf{n}}$ calculated charge distribution in CRD structure at $\lambda = 820$ nm.

Chapter 3

Tuning the resonances to further improve magneto-optical activity.

Chapter 2 presents how the novel exploit of interaction between the dipolar plasmon resonance in a ferromagnetic disk with the S_6 multipolar dark cavity mode of a ring leads to an unprecedented enhancement of the MOA of the cylindrical nanoantenna. In this chapter, we begin to explore how this can be further amplified. The previous content represents a closed result by itself, fruit of the effort of many months. What follows is the sensible continuation, which will take much longer time than this end-of-degree project can afford to span. As such, we will present the first results and ideas devised to explore this newly discovered path.

We already addressed the fact that the resonant peak of the permalloy dot happens at $\sim \lambda = 550$ nm, whereas the S_6 with which it hybridises is estimated to have its largest contribution at $\sim \lambda = 820$ nm. This raises the question of whether the amplification of MOA would be favoured if both resonances occur at the same spectral point. Moreover, one could hope for a ferromagnetic material that produces a comparable (or even better) MO signal to that of permalloy, but sustaining a sharper, stronger plasmonic resonance.

There are multiple ways the resonance of the disk could be tuned to that of the ring. One straightforward manner would be to vary both the radius of the dot and its thickness. Furthermore, the geometrical parameters of the ring could be adjusted to bring the resonances closer. Here, as a first approach, we explore the effects that this tuning could have in the enhancement of MOA by means of computer simulations modifying the dielectric function of permalloy to tailor a sharper dipolar plasmon in the disk positioned at points surrounding the S_6 resonance of the nanocavity. This would yield the results necessary to assess whether investing more time in realising this kind of tuned system is worth the effort.

3.1 Tuning the disk resonance

According to the *Frölich condition*, the permittivity of a metal (ε_m) and the surrounding environment (ε_{env}) must satisfy the relation $\mathrm{Re}\,\varepsilon_m = -2\varepsilon_{env}$ for a plasmonic resonance to occur. With this in mind, we first decrease the imaginary part of the dielectric function of permalloy in order to obtain a sharp resonance. After that, $\mathrm{Re}\,\varepsilon_m$ is adjusted so the intersection with $-2\varepsilon_{env}$ occurs at the desired wavelength (Fig. 3.1). Since the embedding medium is not homogeneous, it is not possible to compute that point of intersection manually. We resort to the analytical expressions of the polarisation of a general ellipsoid (Ref. [22]) implemented in *Wolfram Mathematica* to numerically calculate where the resonance happens for an oblate spheroid of radius 50 nm and height 40 nm, which closely resembles the cylindrical disks, embedded
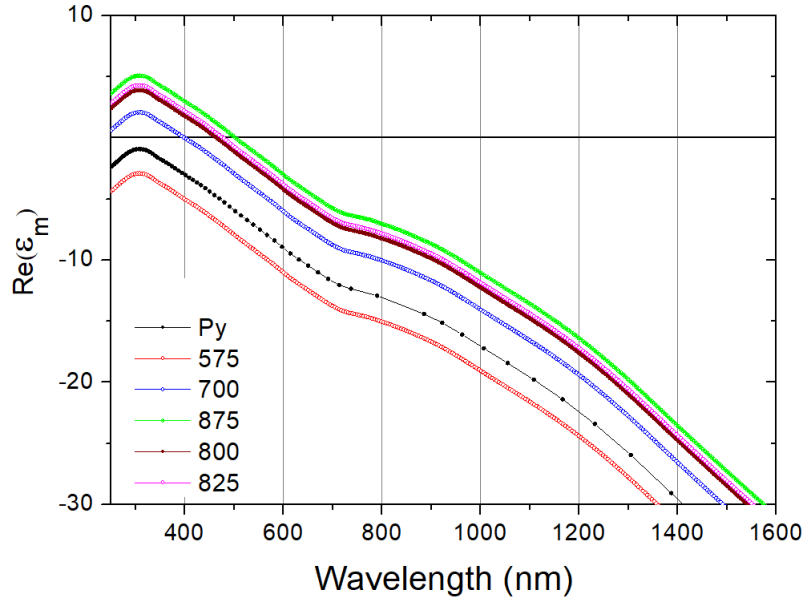
FIGURE 3.1: Modified real part of permalloy dielectric function. Labels represent where the resonant peak occurs according to COMSOL simulations.

in a medium of refractive index the average of the substrate and air (approximately 1.35). This provides a quick reference of where the resonance may happen.

Next, the array of $R_d = 50$ nm dots is modelled in COMSOL's port formulation following the guidelines of Appendix A, in this case keeping the pitch of the lattice at 1000 nm to prevent diffraction coupling from occurring in the range around 800 nm of incoming wavelength. In ideal conditions one would want the peaks in figure 3.2a to share the same maximum value, which is not the case. The method used here is a first approach and does not provide this level of fine tuning but results should not be ambiguous noting which dielectric functions yield slightly higher signals. Furthermore, small peaks appear at around $\lambda = 600$ nm in some cases. This is yet to be explained but could be a product of the modification of ε_m. Nevertheless, they lie outside the range of interest around the S_6. We know these peaks do not correspond to higher diffractive coupling orders because they do not appear at the expected values of λ. Figure 3.2b shows that broader, less intense resonances can be achieved by increasing the imaginary part of ε_m.

3.2 Optical response in NCRD system

Each of the previous dielectric functions for dots is systematically used in a NCRD system in ports formulation to explore their effect in the optical response. The geometry used in this case is $R_i = 125$ nm and $R_o = 225$ nm for the ring. The whole structure is 40 nm thick and the gap is $g = 15$ nm.

Due to variations in the parameters of the ring with respect to Chapter 2, the S_6 resonance is now taking place at $\lambda = 750$ nm approximately. This is further confirmed by the peak at that exact point that NCRD with disk resonating near that point have according to figure 3.3. This graph shows that the feature at that wavelength is more pronounced for the dot tuned at $\lambda = 700$ nm. A similar signal value is achieved by the dot tuned at $\lambda = 575$ nm although the former is the strongest resonance judging by fig. 3.2a and the latter, the weakest. This hints at the best coupling
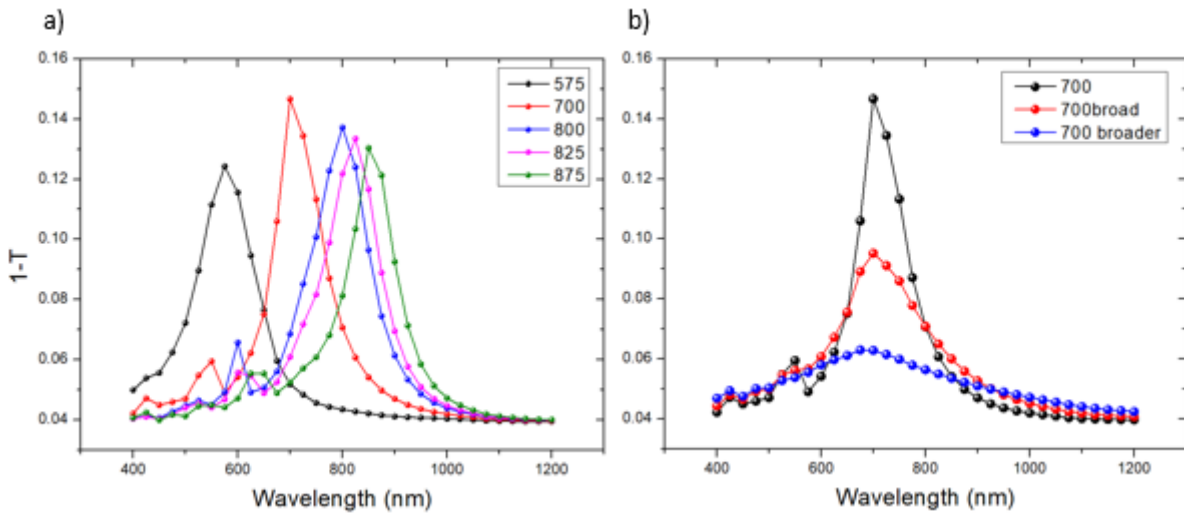
FIGURE 3.2: a)1-Transmittance of different dielectric functions computed in ports formulation in COMSOL. Labels mark the where the maximum happens.b) 1-T of dots of dielectric functions with different imaginary part.
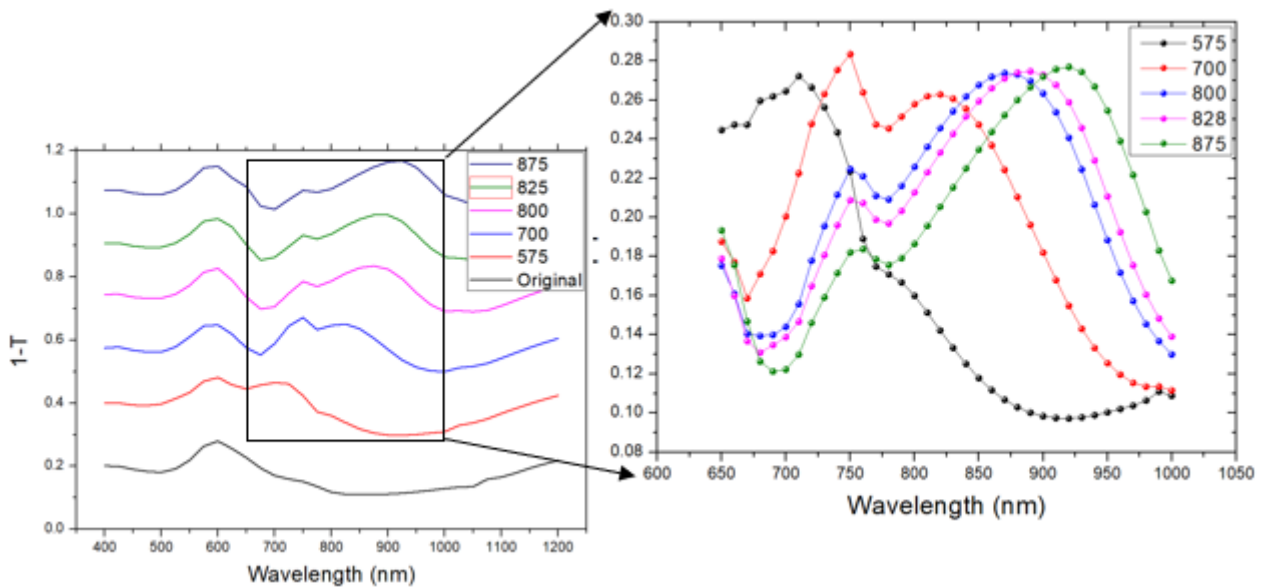
FIGURE 3.3: 1-Transmittance lineshapes for NCRD systems containing dot with different artificially adjusted dielectric functions and original permittivity (used throughout the text for permalloy from ref. [19]). Zoom-in graph of 650 nm - 1000 nm range for artificial dots.
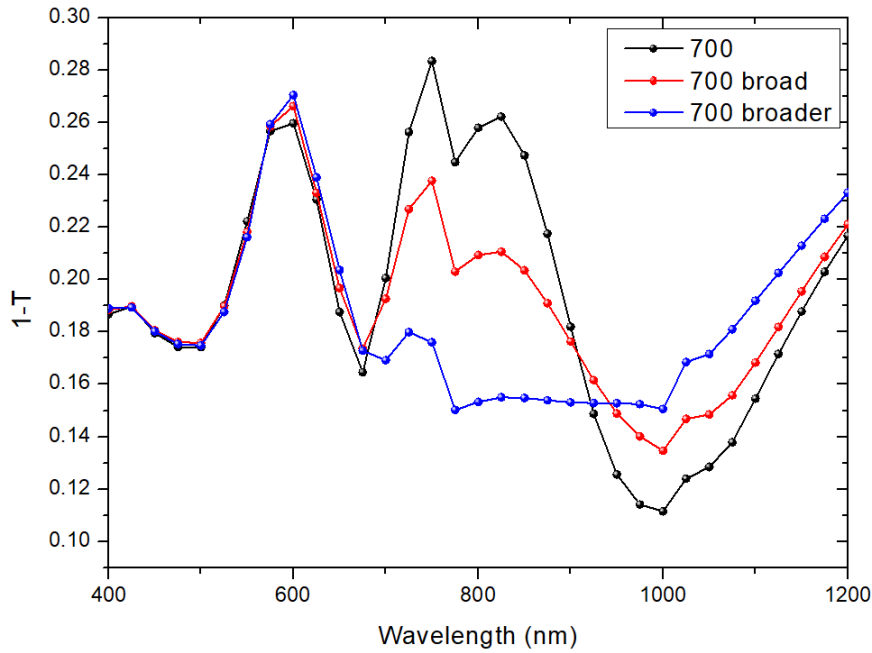
FIGURE 3.4: 1-Transmittance of NCRD with dot tuned at 700 with increasing loss level attributed to an increased imaginary part of the dielectric function.

to S_6 cavity mode being for the dot tuned at $\lambda = 700$ nm. Consequently, a deeper analysis is made at that point (Fig. 3.4).

Intuitively, as the resonance gets weaker, so does the coupling with the octupolar mode of the ring and, in fact, both the signals of the standalone dot and hybrid mode of NCRD are reduced approximately by the same value as the loss in the "artificial material" increases. This suggest that, indeed, a stronger resonance makes the situation more favourable as far as optical response is concerned. The peak at $\lambda = 600$ nm does not vary appreciably and is attributed almost exclusively to the *super-radiant* anti-bonding mode of the ring. The rest of the shape corresponds to a smoother peak which is red-shifted along with the resonance of the disk. What is remarkable is that this peak appears at longer wavelengths than the plasmon of the standalone disk, e.g., for the red curve this second maximum appears at ~ 820 nm whereas figure 3.2 shows that the resonance occurs at around 700 nm. This two-peak structure was not present in the case studied on Chapter 2 and requires further research.

Magneto-optical measurements are not implemented in this model. A way of correctly modifying the off-diagonal terms in the dielectric tensor 1.27 is necessary in order to enable the MO response of the system. This can be done by substituting the modified ε in expression 1.27, keeping the Voigt parameter as it is. Simulations including this effects are planned but out of the scope of this text due to time constraints.

However, one can still speculate if a MOA enhancement is expected by comparing the change in transmittance and optical dipole strength between the real permalloy and the "tuned" material in figure 3.5. Subfigure 3.5a shows that dipole strength, which is proportional to $|\sigma|_{max}$ is more than quadrupled in the case of the sharper, tuned resonance (actual ratio of ~ 4.45) while 3.5b reveals that the ratio of 1-T is only ~ 1.78. This means that a MOA enhancement is possible although the ratio between
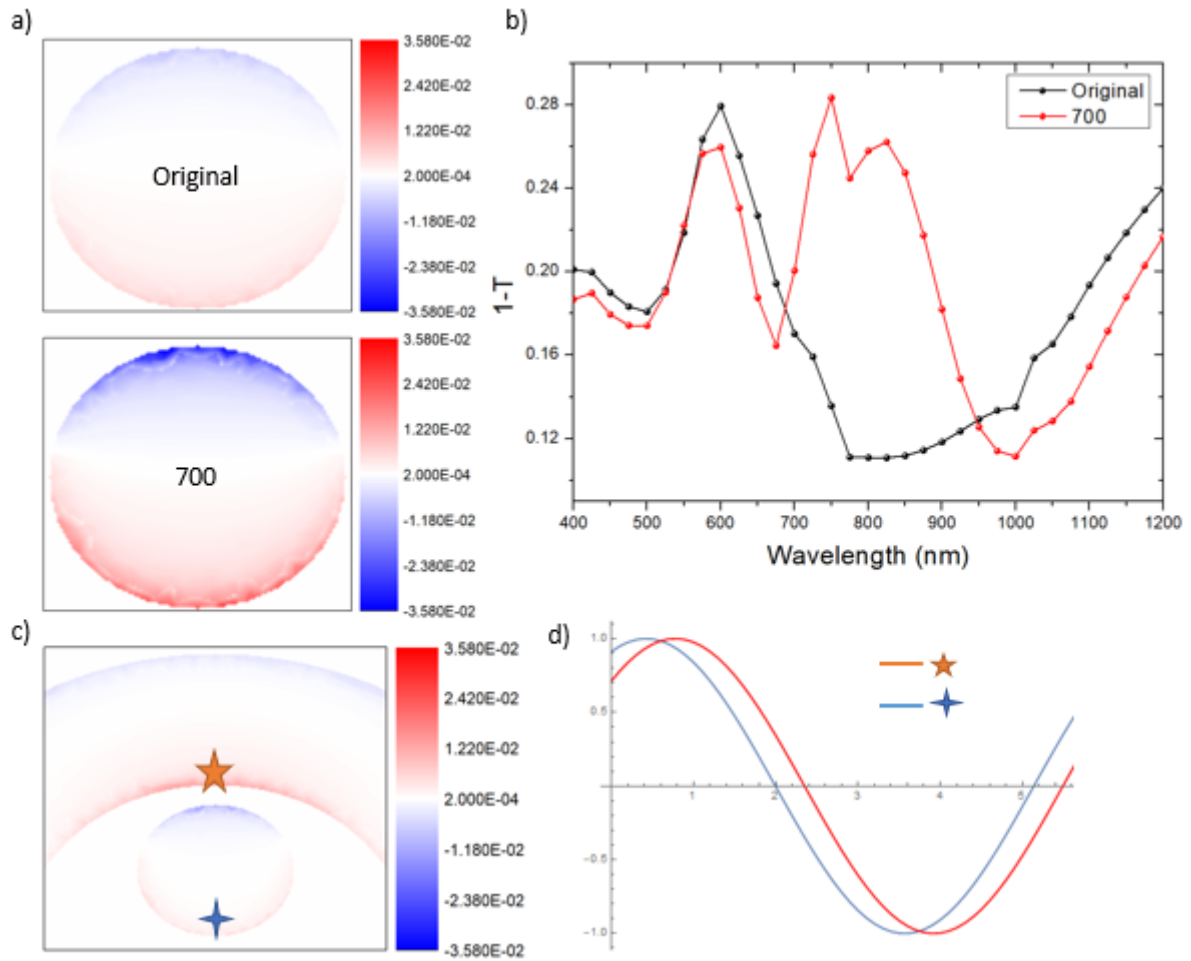
FIGURE 3.5: Comparison between original permalloy and tuned material disks in NCRD system at $\lambda = 750$ nm. a) Dipole charge distribution for sharpest dot tuned at $\lambda = 700$ nm and original Py ($\lambda \approx 550$ nm) computed through normal component of the real part of polarisation. b) Calculated 1-Transmittance for NCRD systems containing the disks in (a). c) Dipole contribution after subtracting S_6 charge distribution from ring alone d) Normalised charge distribution at points marked in (c) evolving in time and relative phase of dipole in ring and disk.

the optical dipole and the MOLPR one must be considered.

Chapter 4

Conclusion

4.1 Summary

The work here described shows that the enhancement of the magneto-optical activity in ferromagnetic nanoantennas, in this case permalloy disks, through localised plasmon resonances may be pushed beyond the current limit by using multipolar dark nanocavity modes of a plasmonic ring when both components are arrange in a way that the circular symmetry of the system is broken. The off-centred position of the Py dot inside the nanocavity allows the excitation of said multipolar modes by incoming linearly polarised light. Namely, the *octupolar* mode of the ring, which is *low-radiant*, hybridises with the dipolar, bright, *radiant* mode of the disk resulting in a *radiant* magneto-optical dipole driven by an optical one that is not largely increased. The ratio of the two dipoles, which gives the magneto-optical activity, is thus extraordinarily enhanced up to approximately 1 order of magnitude with respect to the bare nanoantenna. Furthermore, this response can be tailored to specific applications, in flat optics and sensing for example, by modifying the geometrical parameters of the hybrid structure and the constituent materials.

We have also explored how the tuning of the disk resonance, which takes place in a spectral position distant to that of the octupole, may induce a stronger response and a even larger enhancement of the magneto-optical activity. In a purely theoretical way, we have modified the dielectric function of permalloy in order to shift the spectral position and increase its sharpness and strength. These first results, pertaining only to the optical response, shows that the interaction is favoured by a stronger plasmonic resonance in the disk as one would expect.

4.2 Outlooks

This exploratory work opens a path for future research to further analysis and practical use of these kind of interactions. The amplified electrodynamics in the ferromagnetic disk might be utilized to achieve an efficient injection of optically-induced spin-polarized hot electrons in spintronic devices and have a huge impact on forthcoming photonic nanotechnologies based on plasmon-mediated local enhanced manipulation of electronic spin-currents opening excellent perspectives in disclosing novel opto-electronic phenomena.

Regarding the effect of tuning the resonances, further research must be done in order to get conclusive results. We propose the continuation through this computational/theoretical path as a first approach which has to be complemented with a method to change the magneto-optical response of the system along with the optical part to get the full picture of the interaction. This might be achieved by properly

modifying the off-diagonal terms in the dielectric tensor to conform to the new properties of the "artificial" material.

Appendix A

Details on COMSOL simulations

A.1   Equipment

Simulations run on a Lenovo ThinkStation equipped with an Intel®Xeon®CPU ES-1650 v3 at 3.5 GHz and 128Gb of RAM memory running Windows®7 Professional (Service Pack 1). COMSOL®Multiphysics version is 5.2.

A.2   Array modelling for optical computations in *ports formulation*

We use the *RF - Electromagnetic wave* module in *Frequency domain* configuration. Periodic boundary conditions in the XY plane are defined for the square unit cell in figure A.1, matching the opposite faces in the rectangular prism that defines the physical domain. A finely meshed plane of 5 nm thick (max. element size of 15 nm) is placed at around 2λ in order to measure the fields for MO calculations, which is currently not used as SFF is more suitable for the moment (may be removed to shorten computation times). To prevent wave reflections at domain boundaries, two PML are placed, meshed with quadrilateral swept finite elements. Physical domain boundaries are meshed in standard *free triangular*. The remaining geometry is meshed with *free tetrahedral* elements of various maximum sizes. Active area is finely meshed while distant air and substrate domains have maximum element size below the recommended $\lambda/10$.

Optical constants are introduced through interpolation of tabulated data and definition of diagonal permittivity tensor [17] [19]. Reflectivity and transmittance are computed with the COMSOL-available quantities of reflected and transmitted power (absolute value squared of `emw.S11` and `emw.S12` with two ports, port No.1 being where the excitation occurs).

The number of finite elements is kept at around 200 thousand, averaging a computation time of 10 minutes per point depending on whether dot or NCRD (more fine elements) arrays are being modelled.

A.3   Single structure MOA and optical modelling in *Scattered field formulation*

Same *RF - Electromagnetic wave* module in *Frequency domain* configuration. The physical domain is a rectangular prism surrounded of PML layers to prevent reflections (Fig. A.2). The model resizes according to the incoming wave parametrised by wavelength λ to ease computation load. A "monitor" cylinder is placed to calculate the electric field values. The structure is lain inside a finely tetrahedrally meshed
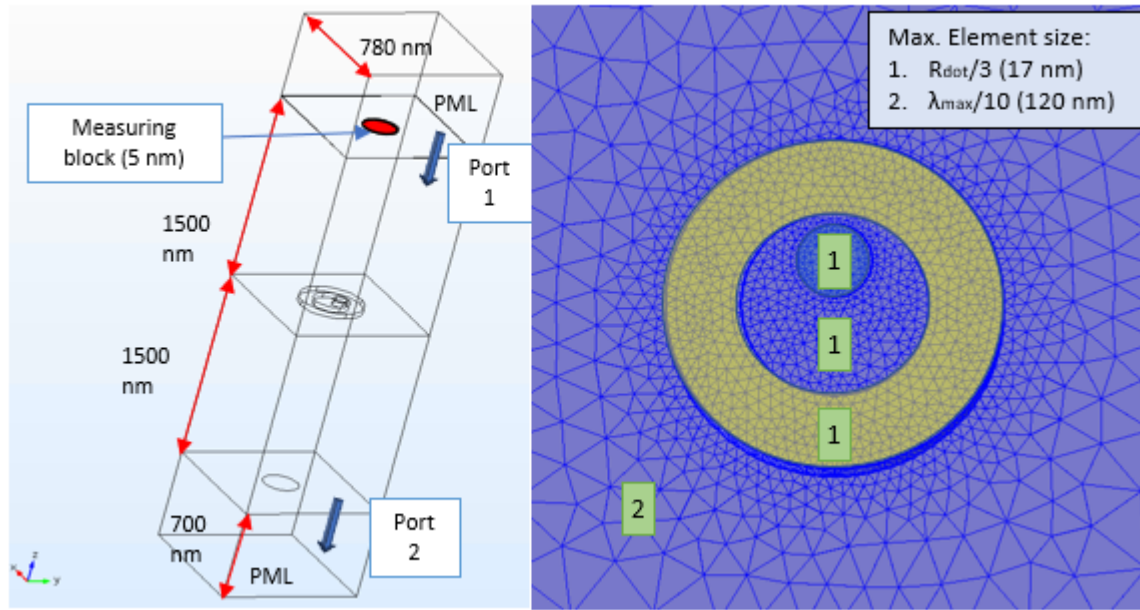
FIGURE A.1: Geometry and meshing of the physical domain and active area of the ports formulation model used to compute reflectivity and transmittance. Port 1 excites the incoming wave (direction marked with blue arrow).
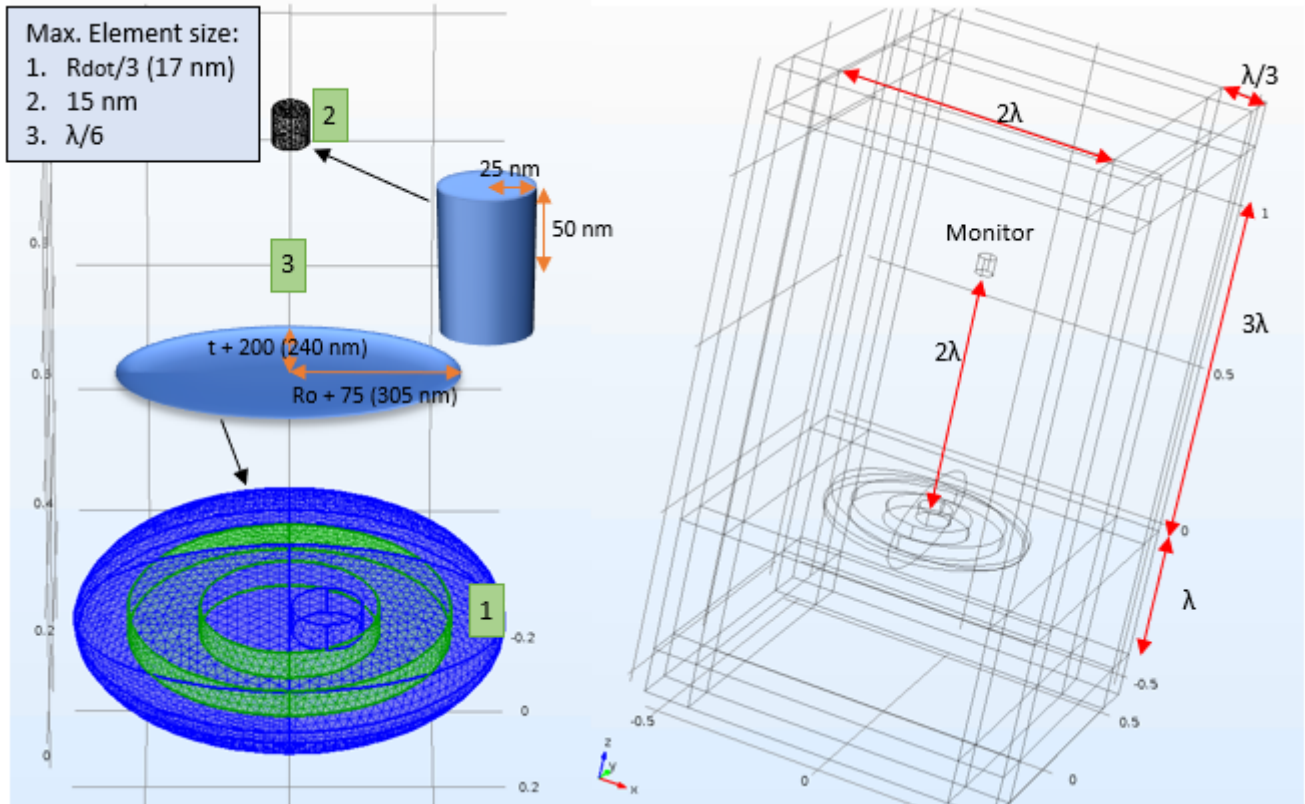
FIGURE A.2: Geometry and meshing of the physical domain and active area of SFF model used to compute MO quantities cross-sections.

elliptical enclosure. PML layers are *swept-meshed* with quadrilateral elements. The rest is discretised with *free triangular* elements, air and substrate block with $\lambda/6$ max. size, the enclosure $R_o/3$ and the monitor 10 nm, with R_o the outer radius of the ring.

Electromagnetic field is calculated by defining probes for both real and imaginary parts of E_y and E_x inside the monitor and using the formulas 2.1 in Chapter 2. The absorption and scattering cross-sections are computed by integrating over the enclosure ellipsoid surface the following expressions

- relative Poynting vector: `nx*`*emw*`.relPoavx + ny*`*emw*`.relPoavy + nz*`*emw*`.relPoavz`

- Poynting vector: `nx*`*emw*`.Poavx + ny*`*emw*`.Poavy + nz*`*emw*`.Poavz`

- σ_{sc}: integrate *relative* Poynting vector over enclosure surface and normalise to incoming intensity

- σ_{abs}: integrate Poynting vector over enclosure surface and normalise to incoming intensity

where the relative entities are available in COMSOL and correspond to the quantities apart from the external incoming wave after the interaction with the system.

Computation time varies depending on the incoming field's wavelength, although not abruptly since the finely meshed area remains untouched, averaging 20 minutes per spectral point in our equipment.

Bibliography

[1] N. M. Neil W. Ashcroft, *Solid state physics* (Cengage Learning, Inc, Jan. 2, 1976), 848 pp.

[2] M. G. Blaber, M. D. Arnold, and M. J. Ford, The Journal of Physical Chemistry C **113**, 3041 (2009).

[3] S. A. Maier, *Plasmonics* (Springer-Verlag GmbH, May 2007).

[4] J. D. Jackson, *Classical electrodynamics* (John Wiley & Sons Inc, July 27, 1998), 832 pp.

[5] C. F. Bohren and D. R. Huffman, *Absorption and scattering of light by small particles*, en, Google-Books-ID: S1RCZ8BjgN0C (Wiley, 1983).

[6] M. Meier and A. Wokaun, Optics Letters **8**, 581 (1983).

[7] M. Freiser, IEEE Transactions on Magnetics **4**, 152 (1968).

[8] G. R. Fowles, *Introduction to modern optics* (DOVER PUBN INC, June 1, 1989), 336 pp.

[9] G. Armelles, A. Cebollada, A. García-Martín, and M. U. González, Advanced Optical Materials **1**, 10 (2013).

[10] N. Maccaferri, A. Berger, S. Bonetti, V. Bonanni, M. Kataja, Q. H. Qin, S. v. Dijken, Z. Pirzadeh, A. Dmitriev, J. Nogués, J. \AAkerman, and P. Vavassori, Physical Review Letters **111** (2013).

[11] N. Maccaferri, L. Bergamini, M. Pancaldi, M. K. Schmidt, M. Kataja, S. van Dijken, N. Zabala, J. Aizpurua, and P. Vavassori, Nano Letters **16**, 2533 (2016).

[12] F. Hao, E. M. Larsson, T. A. Ali, D. S. Sutherland, and P. Nordlander, Chemical Physics Letters **458**, 262 (2008).

[13] J. Aizpurua, P. Hanarp, D. S. Sutherland, M. Käll, G. W. Bryant, and F. J. G. d. Abajo, Physical Review Letters **90** (2003).

[14] W. Yan, R. Faggiani, and P. Lalanne, Physical Review B **97** (2018).

[15] A. D. Rakić, A. B. Djurišić, J. M. Elazar, and M. L. Majewski, Applied Optics **37**, 5271 (1998).

[16] F. Hao, P. Nordlander, M. T. Burnett, and S. A. Maier, Physical Review B **76** (2007).

[17] P. B. Johnson and R. W. Christy, Physical Review B **6**, 4370 (1972).

[18] Y. H. Fu, J. B. Zhang, Y. F. Yu, and B. Luk\textquotesingleyanchuk, ACS Nano **6**, 5130 (2012).

[19] Š. Višňovský, V. Pařízek, M. Nývlt, P. Kielar, V. Prosser, and R. Krishnan, Journal of Magnetism and Magnetic Materials **127**, 135 (1993).

[20] T. H. J. Loughran, P. S. Keatley, E. Hendry, W. L. Barnes, and R. J. Hicken, Optics Express **26**, 4738 (2018).

[21]   Y. Sonnefraud, N. Verellen, H. Sobhani, G. A. E. Vandenbosch, V. V. Moshchalkov, P. V. Dorpe, P. Nordlander, and S. A. Maier, ACS Nano **4**, 1664 (2010).

[22]   N. Maccaferri, J. B. González-Díaz, S. Bonetti, A. Berger, M. Kataja, S. van Dijken, J. Nogués, V. Bonanni, Z. Pirzadeh, A. Dmitriev, J. Åkerman, and P. Vavassori, Optics Express **21**, 9875 (2013).